NASA-TP-2564 19860015697

NASA
Technical
Paper
2564

May 1986

Theoretical Three- and Four-Axis Gimbal Robot Wrists

L. Keith Barker
and Jacob A. Houck

NASA

Theoretical Three- and Four-Axis Gimbal Robot Wrists

L. Keith Barker
and Jacob A. Houck

Langley Research Center
Hampton, Virginia

Summary

The most popular method of controlling a robot hand is for an operator to command the hand to move with a velocity in the desired direction. Such control is familiar to pilots of aircraft or spacecraft. This paper deals specifically with rotation of the robot hand by the robot wrist in response to a rotational velocity command from an operator. There is no translational motion of the robot hand. Two major obstacles to rotating the hand with the wrist are (1) joint angle limitation, which is a design problem not considered herein, and (2) the occurrence of excessive joint angle rates at the wrist singularity, which is the focus herein.

Three- and four-axis gimbal systems from flight simulations are discussed with respect to robot wrists, and pertinent equations are assembled. A true three-axis robot wrist is modelled as a three-gimbal system for analysis and is subjected to a basic test maneuver which encompasses the troublesome "gimbal lock" that occurs when two of the rotational axes become colinear. In flight simulations, quaternions are used to calculate gimbal angles in response to pilot inputs to avoid the mathematical singularity associated with gimbal lock. This same approach is used herein. Mechanically, however, implementation of the calculated gimbal angles can still induce excessive gimbal angle rates. Consequently, for the three-gimbal robot wrist, the gimbal angle rates are scaled when necessary so that the robot hand moves in the desired direction but at a slower rate, to prevent limiting of gimbal angle rate. Unfortunately, scaling introduces an undesirable time delay in the robot-hand rotation compared with the actual commanded rotation.

The four-axis gimbal system was designed for flight simulations and is currently used to allow all possible rotations with acceptable gimbal angle rates while it avoids gimbal lock. A hypothetical robot wrist, functionally equivalent to the four-axis gimbal system, is compared with the three-gimbal wrist in the basic test maneuver. The four-gimbal wrist is mechanically more complex than the three-gimbal wrist because of the fourth gimbal angle. But the fourth gimbal angle keeps the robot wrist away from the gimbal lock position while the robot hand moves as commanded. In an extension of the basic test maneuver (to represent a "worst-type" condition for the four-gimbal wrist), it was found that if the robot wrist can rotate at least twice the commanded robot-hand rate, then no scaling is required.

Introduction

A true three-axis robot wrist has, by defini-tion, rotational capability about each of three mutually perpendicular axes, all passing through a single point. Such wrists are, at present, rare (ref. 1). In reference 1, a wrist mechanism with a series of differential bevel gears is suggested as a true three-axis robot wrist. In reference 2, a versatile space manufacturing manipulator is proposed that has an Euler angle wrist configuration (essentially a three-gimbal wrist) which ensures that inverse kinematic solutions always exist. A unique wrist mechanism with four degrees of freedom recently developed at Oak Ridge National Laboratory has intersecting orthogonal pitch, yaw, and roll axes (these three intersecting axes constitute a true three-axis wrist) with all singularities at the extremities of the ranges of motion for teleoperation (ref. 3).

We assume in this paper that a true three-axis robot wrist is functionally analogous (i.e., has the same basic mathematics) to a three-gimbal system used in early flight simulations. In flight simulations, as the need to simulate highly maneuverable fighter aircraft and spacecraft arose, minimizing the dynamic positioning error due to rate limiting of the gimbal system near singular points had to be considered. Consequently, a four-gimbal system was developed (refs. 4 and 5) and is currently being used in flight simulations (ref. 6) to provide complete rotational freedom of one reference frame with respect to another. That is, the four angles that drive the corresponding four-gimbal system can be kept away from the singular condition to avoid gimbal lock and yet represent all rotations. The purpose of this paper is to compare results for three-gimbal and four-gimbal robot wrists rotating a robot hand. The robot hand is commanded to move (through commanded rotational rates) so that the three-gimbal wrist passes through gimbal lock. These results are pertinent to the design of dexterous robot arms needed for delicate tasks or for operation in close quarters (e.g., handling radioactive material, satellite repair, or surgery).

It should be noted that a four-axis robot wrist is also contemplated in reference 7 (which appeared in the literature during the editorial review stage of this paper). Reference 7 and this paper are certainly complementary with respect to a four-axis robot wrist. In reference 7, joint angles are calculated to produce a specified robot-hand orientation, whereas in this paper, joint angle rates are computed to produce commanded robot-hand rates.

A four-gimbal system has been used successfully for many years in flight simulations to avoid gimbal lock. However, researchers in robotics may not be aware of this fact, because there does not appear to be any reference to this implementation.

We hope this paper will aid in a transfer of this technology.

Symbols

a_i	quaternion parameters $(i = 1, 2, 3, 4)$
$a_{i,k}$	quaternion a_i at time t_k
$a_{i,o}$	initial values for $a_{i,k}$
$b_{i,o}$	intermediate parameter used in quaternion initialization
$\mathbf{C}$	transformation matrix from robot-wrist axes X_W, Y_W, and Z_W to robot-hand axes X, Y, and Z
$\mathbf{C}_{k+1}$	matrix $\mathbf{C}$ with elements computed at time t_{k+1}
$C_1, C_2', H,$ $G, J, N, K,$ ρ_k, ω_k	intermediate variables (see fig. 2(c))
c_{ij}	elements of $\mathbf{C}$
F	scale factor to prevent gimbal rate limiting
h	integration step size
K	gain constant
k	integer that refers to time t_k
l_x, l_y, l_z	probe-tip coordinate along X, Y, and Z, respectively
$M(1), M(2), M(3)$	operational limit specified for $\dot{\psi}$, $\dot{\theta}$, and $\dot{\phi}$, respectively
p, q, r	rotational rate about X, Y, and Z, respectively (input by operator)
p_k, q_k, r_k	p, q, and r at time t_k
t	time
t_k	discrete time equal to k integration steps, kh
X, Y, Z	robot-hand axis system
X_W, Y_W, Z_W	robot-wrist axis system
X_F, Y_F, Z_F	robot-forearm axis system
$x_{\text{tip}}, y_{\text{tip}}, z_{\text{tip}}$	probe-tip coordinate along X_F, Y_F, and Z_F, respectively
δ_θ	small positive number to define singularity region
$\lambda(1), \lambda(2), \lambda(3)$	amount by which ψ, θ, and ϕ exceeds its respective specified operational limit $M(1)$, $M(2)$, and $M(3)$
$\psi, \theta, \phi, \alpha$	gimbal angles

A dot over a symbol indicates the first derivative with respect to time.

Analysis

In flight simulations, an airplane or spacecraft has a fixed set of body axes. Likewise, a robot hand can be considered a moving axis system. In the former, rotation is simulated by using gimbal systems; in the latter, rotation is the result of joint movements in the robot wrist.

Three-Gimbal Robot Wrist

Figure 1 illustrates the three-gimbal system described in references 4 and 5 applied to a robot hand instead of to an airplane. The axes X_F, Y_F, and Z_F represent the robot forearm and remain fixed relative to any changes in the gimbal angles ψ, θ, and ϕ (where ψ is about Z_F). The axes X_W, Y_W, and Z_W are the robot-wrist axes; X, Y, and Z are the robot-hand axes. The three axis systems are shown displaced in figure 1, but in this analysis, they are aligned and have a common origin for simplicity. The X-axis is the approach direction of the robot hand, which is shown perpendicular to the robot forearm in figure 1(a). Airplane axis systems are used for easy transition from references 4 and 5 to this paper. An operator commands the rotational rates p, q, and r about the hand axes. The robot-wrist gimbal angles ψ, θ, and ϕ then change so that the robot hand moves at these commanded rates.

The well-known equations that relate $\dot{\psi}$, $\dot{\theta}$, and $\dot{\phi}$ to p, q, and r are shown in figure 1(b) for reference. In robotics, such equations are called resolved-rate equations. These equations can be integrated to get the gimbal angles, although this is not usually done in flight simulations of highly maneuverable aircraft or spacecraft. Rather, quaternion rate equations (which are never singular) are used to calculate the gimbal angles.

Rotation of one reference frame at rates p, q, and r with respect to another can be described by using either gimbal angles (usually called Euler angles), direction cosines, or quaternions. Comparing terms in the resultant transformation matrices (which must be equivalent) establishes the relationships between

the quaternions and the gimbal angles shown in figure 1(c). The widely used algorithm developed in reference 8 is later used to integrate the quaternion rate equations.

Discrete Equations for Three-Gimbal Wrist

The block diagram in figure 2(a) shows an overview of the discrete equations for the three-gimbal wrist. A subscript k corresponds to the time $t_k = kh$, and the subscript $k + 1$ refers to the next update time $t_{k+1} = t_k + h$, where h is the integration step size. Given p_k, q_k, and r_k, the objective is to calculate the next set of gimbal angles ψ_{k+1}, θ_{k+1}, and ϕ_{k+1}. Note that the gimbal angle rates are not actually needed to compute the gimbal angles. Subsequently, a scaling procedure is described which does use the rates to modify the operator inputs p_k, q_k, and r_k so that no gimbal rate exceeds its operational limit.

The individual blocks in figure 2(a) are shown expanded in figures 2(b) to 2(g). Block 1 is expanded in figure 2(b), in which initial values of the quaternions that correspond to the initial gimbal angles ψ_o, θ_o, and ϕ_o are given by $a_{i,o}$ ($i = 1, 2, 3, 4$). Block 2 in figure 2(c) shows the algorithm for updating the quaternions as a function of the operator inputs p_k, q_k, and r_k. This algorithm is given in reference 8 as a possible simplified version (i.e., no feedback of $\dot{p}$, $\dot{q}$, and $\dot{r}$) of a more general algorithm that is derived for flight simulations. Block 3 is shown in figure 2(d), in which the updated quaternions are used to compute the updated transformation matrix $\mathbf{C}_{k+1}$ (ref. 8). Block 4 in figure 2(e) transforms the probe-tip coordinates from the hand axis system to the wrist axis system through use of the updated transformation matrix $\mathbf{C}_{k+1}$. Block 5 in figure 2(f) shows how the updated gimbal angles ψ_{k+1}, θ_{k+1}, and ϕ_{k+1} are computed from the elements of the transformation matrix $\mathbf{C}_{k+1}$. Finally, block 6 in figure 2(g) gives equations for computing the gimbal angle rates. These rates are not used to compute the gimbal angles, but they are later scaled so that no gimbal rate exceeds its operational limit. No scaling is indicated in figure 2.

Scaling Excessive Gimbal-Angle Rates

Scaling away from singularity. The gimbal angles are not computed by integrating the gimbal angle rates, but the rate equations remain valid and can still be used for scaling purposes away from the singularity. Figure 3(a) shows this scaling procedure. The gimbal angle rates are computed. Then, through the λ-equations, each rate is compared with its maximum allowable rate. If any rate exceeds its limit,

then all rates are scaled by the scale factor F so that the gimbal angle rate that most exceeds its limit is scaled to its maximum value, maintaining the same sign as the computed rate that is being scaled. The operator inputs are similarly scaled by F before they are used to update the quaternions for subsequently calculating the updated gimbal angles. What this means is that if the gimbal angle rates are scaled, the robot hand still rotates in the commanded direction, but slower than originally commanded.

Scaling at singularity. The gimbal-angle-rate equations are not defined when $\cos \theta = 0$, and the rates can become extremely large very close to this singularity. Consequently, a special method for scaling the gimbal angle rates is used whenever $|\cos \theta| < \delta_\theta$, where δ_θ is a small specified positive number. Herein, $\delta_\theta = 0.001$. An overview of calculations for the singularity region is given in figure 3(b). All the numbered blocks have been previously described. Average gimbal angle rates are defined by the difference between the updated gimbal angle and the current gimbal angle divided by the integration step size h. These average rates can then be scaled as in figure 3(a). If the rates are scaled, then the updated gimbal angles are recomputed as the current value plus the scaled rate times the integration step size. Afterwards, updated quaternions are computed that correspond to these updated gimbal angles. This method of scaling allows the robot hand to move through the robot-wrist singularity condition ($\cos \theta = 0$); however, the adverse effect of scaling is a delay or pause in the movement of the robot hand with respect to the commanded movement. Hence, for certain tasks, scaling may be intolerable. The merit of the four-gimbal wrist is that the singularity condition is never encountered.

Basic Test Maneuver

Assume a 6-in. probe in the robot hand initially lies along X or X_W in figure 1(a). A basic test maneuver is defined as moving the tip of the probe through the ordered sequence of points (6,0,0), (0,0,−6), and (0,6,0) with respect to the robot-forearm axis system X_F, Y_F, and Z_F. That is, the probe rotates about Y from the initial horizontal position (6,0,0) to the vertical position (0,0,−6) and is then rotated to point along Y_F with coordinates (0,6,0). This is a difficult maneuver for a three-gimbal wrist because the equations for figure 1(a) are indeterminant for the vertical tip position and, near this position, very large rates are computed.

To perform the basic test maneuver, an operator commands a constant value for rotational rate q

until the probe points vertically and then instantaneously changes the command to a constant value of rotational rate r for the rest of the maneuver. The nominal integration step size is $h = 1/32$ sec. The probe is forced to be located exactly at the vertical position for an integer multiple of h to simulate a "worst-type" condition for the three-gimbal wrist. In the first part of the maneuver, the operator inputs are $p = 0$ deg/sec, $q = 32$ deg/sec, and $r = 0$ deg/sec, so the probe pitches 1° every integration step and, therefore, passes through the vertical position in 90 iterations, or 2.8125 sec. In the second portion of the maneuver, $p = 0$ deg/sec, $q = 0$ deg/sec, and $r = 32$ deg/sec.

The probe-tip coordinates in the robot-wrist axis system are computed as $x_{\text{tip}} = Lc_{11}$, $y_{\text{tip}} = Lc_{12}$, and $z_{\text{tip}} = Lc_{13}$ (fig. 2(e)), where $L = 6$ simulates a 6-in. probe pointing along the X-axis of the robot hand and where the components of the transformation matrix $\mathbf{C}$ are given in figure 1(c).

Four-Gimbal Robot Wrist

Figure 4(a) indicates the use of the four-gimbal wrist to rotate a robot hand. When $\alpha = 0°$, the four-gimbal wrist reduces to the three-gimbal wrist in figure 1(a). As shown in references 4 and 5, the gimbal-angle-rate equations can be expressed as shown in figure 4(b). The order of rotation of the gimbal angles is ψ, θ, ϕ, and α. The basic idea is to use $\dot{\alpha}$ to change the sign on $\dot{\theta}$ before the singularity condition $\cos\theta = 0$ is reached. A function is chosen for $\dot{\alpha}$ so that (1) $\dot{\alpha}$ is always in a direction opposite to $\dot{\theta}$ and (2) the magnitude of $\dot{\alpha}$ becomes large enough to dominate the equation for $\dot{\theta}$ before θ reaches the singularity condition. A simple expression for $\dot{\alpha}$ from reference 4 is

$$\dot{\alpha} = -K \sin\theta \ \text{sgn}(\sin\phi) \qquad (1)$$

where K is a specified positive constant. The value K must be large enough for $\dot{\alpha}$ to dominate $\dot{\theta}$ without inducing excessive gimbal angle rates. Gimbal angles are actually computed by use of quaternion equations (fig. 4(c)).

The block diagram in figure 5 shows the $(k+1)$ iterative solution for the gimbal angles and the probe-tip coordinates for the four-gimbal wrist. The kth gimbal angle rates are also computed for observation. Figure 5(a) presents an overview of the calculations. An operator issues the discrete inputs p_k, q_k, and r_k, which are used to calculate the updated quaternions in block 2. Then, the quaternions are used to calculate elements of a transformation matrix $\mathbf{C}_{k+1}$ in block 3, and the elements are then used to compute

the probe-tip coordinates in block 4 and the updated gimbal angles in block 5 (fig. 5(b)). The details of blocks 2, 3, and 4 are not shown in figure 5 since they are the same as those in figure 2. The quaternions are initialized in block 1 (shown in fig. 5(c)).

Calculation of the updated gimbal angles also requires the updated fourth gimbal angle α_{k+1}, which is obtained from an Adams-Bashforth second-order predictor integration. In figure 5(c), $\alpha_{-1} = \alpha_o$ initiates the α integration with an Euler integration step. The gimbal angle rates are computed in block 6 (fig. 5(d)).

To avoid unnecessary rotations of the four-gimbal robot wrist when there are no operator commands for the robot hand to move (i.e., when $p_k = q_k = r_k = 0$), the condition $\dot{\alpha}_k = 0$ is imposed and α_k is held constant at its past value. This feature is not indicated in figure 5. There are no time periods in the basic test maneuver when all operator inputs are zero.

Results and Discussion

This paper examines the kinematic rotation of the robot hand by its wrist in response to rotational velocity commands from an operator or a computer program. Two robot-wrist configurations are assumed, namely, (1) a true three-axis gimbal robot wrist and (2) a four-axis gimbal robot wrist.

Ideal probe-tip movement is shown in figure 6 for the basic test maneuver. The objective is to rotate the robot hand with a three-gimbal robot wrist and with a four-gimbal robot wrist in an attempt to move the tip of the probe in the robot hand in this prescribed ideal manner.

Three-Gimbal Robot Wrist

Operationally, the joints in a robot wrist can only rotate so fast. However, results are first given with no limits imposed on rotational rates. Results are then given for proportionally scaling the rotational rates such that no rate exceeds its imposed operational limit.

Without scaling. Figure 7 shows the operator inputs, probe-tip movement, gimbal angle rates, and gimbal angles as a function of time when the three-gimbal wrist is used in the test maneuver. Gimbal angle rates are not scaled. The main point of figure 7 is that the gimbal angle rates (fig. 7(c)) are intolerable as the vertical position is approached (at about 2.8 sec). Theoretically, the rates are infinite at $\theta = 90°$. However, if extremely large rates were operationally possible, the probe-tip movement (fig. 7(b))

would agree exactly with the ideal variation in figure 6. At the vertical position of the probe ($\theta = 90°$ in fig. 7(d)), both ψ and ϕ must change instantaneously to 90° to accommodate the second part of the maneuver.

With scaling. As shown in figure 3(a), scaling consists of first computing the gimbal angle rates. If one or more of these rates exceeds an imposed limit of ± 32 deg/sec, the rate which most exceeds this limit is then scaled to equal the limit. The remaining two rates are scaled by the same proportional scale factor. However, gimbal angle rates are not integrated to compute the gimbal angles. Hence, equivalently, the operator inputs are scaled before application by the same amount as the gimbal angle rates to generate the next set of gimbal angles. The effective operator inputs, probe-tip movement, gimbal angle rates, and gimbal angles are shown in figure 8. A comparison of figures 7(b) and 8(b) shows that the probe moves as desired except there is a time delay of about 2.8 sec between parts of the maneuver with scaling. This delay is inversely proportional to the maximum amplitude rate limit; for example, if the limit were halved from ± 32 deg/sec to ± 16 deg/sec, the delay would be twice as long. Operator inputs are scaled to very small values (fig. 8(a)) as ψ and ϕ work their way toward 90° (fig. 8(d)) at the rate limit of ± 32 deg/sec (fig. 8(c)). With scaling, the three-gimbal wrist has the undesirable effect of delaying the response of the robot hand to the commanded movement.

Four-Gimbal Robot Wrist

Figure 9 shows operator inputs, probe-tip movement, gimbal angle rates, and gimbal angles for the four-gimbal robot wrist in the basic test maneuver. Note that the maximum gimbal angle rate (fig. 9(c)) is about 57 deg/sec, which is about 1.8 times the commanded robot hand rate of 32 deg/sec (fig. 9(a)). The maximum magnitude of θ (fig. 9(d)) is about 45°. Probe-tip movement (fig. 9(b)) is the same as the ideal movement shown in figure 6(b).

For the four-gimbal wrist with $K = 0.8$ (eq. (1)), figure 10 shows what happens when the second part of the basic test maneuver is continued. In essence, the probe continues to rotate in the vertical plane (Z_F and Y_F) as indicated in figure 10(b) by the cyclic nature of z_{tip} and y_{tip} with $x_{tip} = 0$. In figure 10(d), ψ and ϕ stay around 90° while θ appears to approach −44°. Meanwhile, α has taken over the basic function of rotating the probe. Correspondingly, as shown in figure 10(c), $\dot{\psi} = \dot{\phi} = 0$ deg/sec, $\dot{\theta} \rightarrow 0$ deg/sec, and $\dot{\alpha} \rightarrow 32$ deg/sec (the commanded probe rotation rate).

Figure 11 shows the magnitude of the maximum gimbal angle rate that occurs in an extension of the basic test maneuver as a function of K and operator input. The upper curve is for operator commands of $q = 32$ deg/sec in the first part of the basic test maneuver and $r = 32$ deg/sec in the second part. Likewise, the lower curve is for constant operator inputs of 16 deg/sec. Notice that $\phi = 90°$ in the second part of the extended test maneuver (fig. 10(d)). In general, when $|\phi| = 90°$, $\dot{\alpha}$ will not dominate the sign of $\dot{\theta}$ (fig. 4(b)) as $|\theta| \rightarrow 90°$ unless $K > |r|$. That is, K must exceed the magnitude of r in radians per second. Therefore, on the curve for 32 deg/sec, $r = 32$ deg/sec and $K > 32\pi/180 = 0.56$ rad/sec. Likewise, on the curve for 16 deg/sec, $K > 0.28$ rad/sec. Extremely large rates are observed for smaller values of K.

If a maximum gimbal angle rate of 32 deg/sec is desired without scaling, then the operator input could be limited to 16 deg/sec with $K = 0.8$. Hence, it appears that the basic test maneuver can be accomplished without scaling the gimbal angle rates if the rates are about twice or more the operator input rates.

Concluding Remarks

Gimbal systems have been used in flight simulations for many years, and the associated technology has direct application to robotics and teleoperator systems. For example, a true three-axis robot wrist is functionally equivalent to a three-axis gimbal system, where the gimbal angles represent joint angles, in that both provide rotational capability about each of three mutually perpendicular axes all passing through a common origin. However, both are plagued by the infamous "gimbal lock" problem. A four-gimbal system is currently used in flight simulations to counteract this problem and yet allow complete rotational freedom. In this paper, theoretical three- and four-gimbal robot wrists are compared in a basic test maneuver that encompasses gimbal lock.

With the three-gimbal robot wrist, scaling must be used because of the wrist singularity to prevent limiting of gimbal angle rates. The major drawback is that scaling, in effect, introduces a time delay in robot-hand rotation with respect to the actual commanded rotation. Depending on what is being done with the robot hand, this delay may or may not be detrimental.

The four-gimbal robot wrist is mechanically more complex than the three-gimbal wrist because of the fourth gimbal angle, but the fourth gimbal angle keeps the robot wrist away from the wrist singularity so that the robot hand always moves exactly as

commanded. It was found that in a "worst-type" maneuver of the robot hand, the fourth gimbal angle could be defined so that none of the gimbal angle rates exceeded twice the commanded rates.

NASA Langley Research Center
Hampton, VA 23665-5225
February 21,1986

References

1. Robots—Prospects for Progress. *Engineering,* July/Aug. 1984, pp. 521–523.
2. Wallace, R. S.; and Gowdy, J. N.: Robotics and the Space Station. *1984 ASME International Computers in Engineering Conference and Exhibit,* American Soc. Mech. Eng., 1984, pp. 369–373.
3. Hamel, W. R.; Feldman, M. J.; and Martin, H. L.: Advanced Teleoperation in Nuclear Applications. *1984 ASME International Computers in Engineering Conference and Exhibit,* American Soc. Mech. Eng., 1984, pp. 302–305.
4. Wilson, John W.: *Analysis and Mechanization of Three- and Four-Gimbal Systems.* NASA TN D-4689, 1968.
5. Wilson, John W.: Four-Gimbal Systems for Simulation Display. *Simulation,* vol. 12, no. 3, Mar. 1969, pp. 115–120.
6. Ashworth, B. R.; and Kahlbaum, William M., Jr.: *Description and Performance of the Langley Differential Maneuvering Simulator.* NASA TN D-7304, 1973.
7. Stanišić, Michael M.; and Pennock, Gordon R.: A Nondegenerate Kinematic Solution of a Seven-Jointed Robot Manipulator. *Int. J. Robot. Res.,* vol. 4, no. 2, Summer 1985, pp. 10–20.
8. Barker, Lawrence E., Jr.; Bowles, Roland L.; and Williams, Louise H.: *Development and Application of a Local Linearization Algorithm for the Integration of Quaternion Rate Equations in Real-Time Flight Simulation Problems.* NASA TN D-7347, 1973.
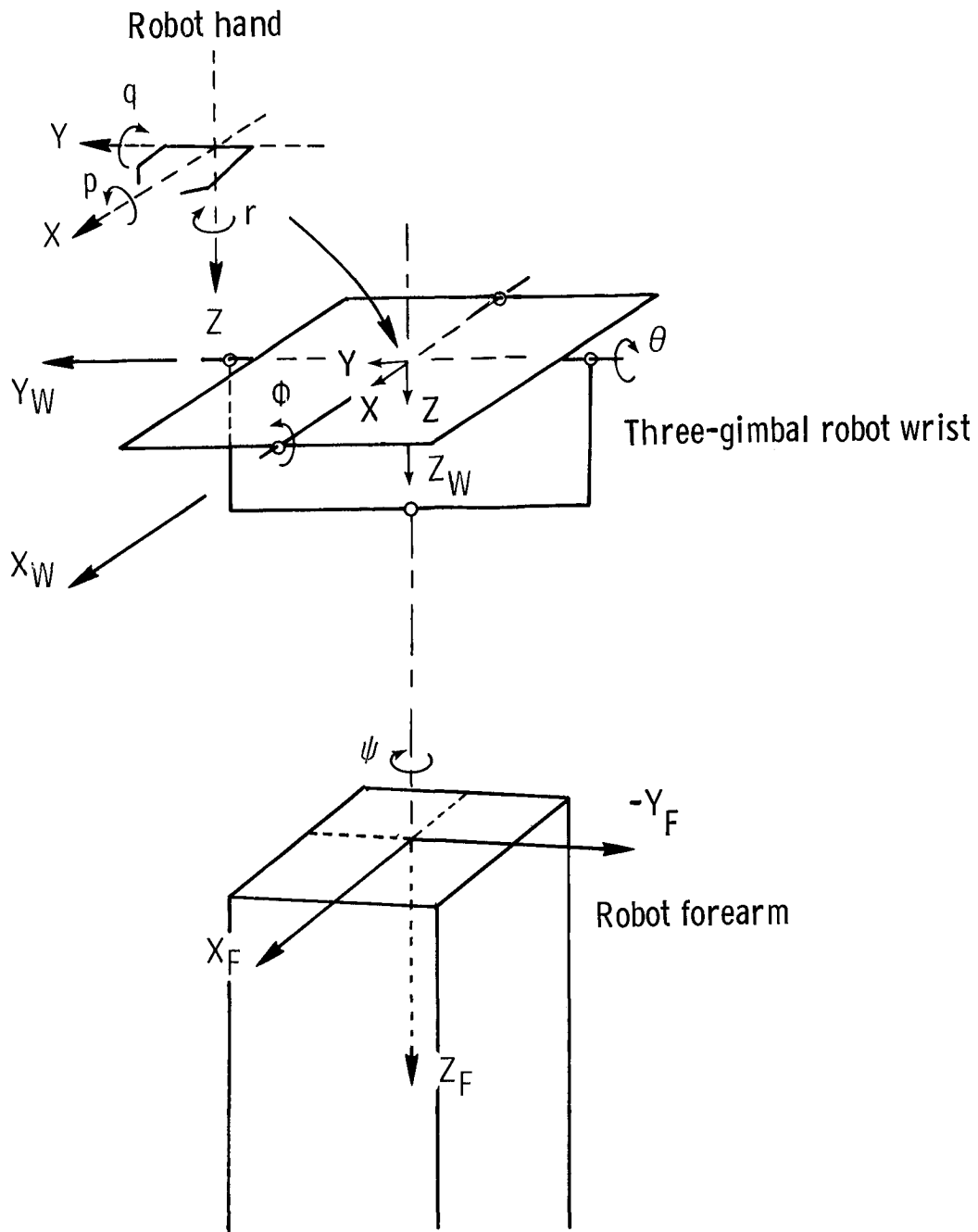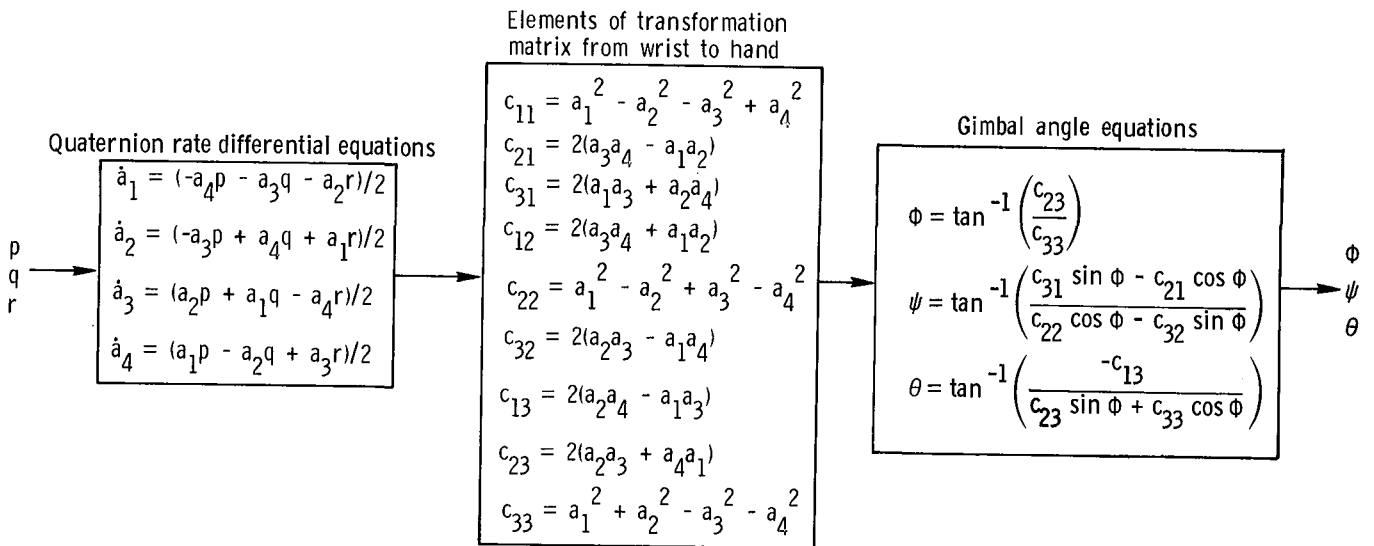
(a) Axis systems.

Figure 1. Robot hand with three-gimbal robot wrist.

$$\dot{\psi} = \frac{r \cos \Phi + q \sin \Phi}{\cos \theta}$$

$$\dot{\theta} = q \cos \Phi - r \sin \Phi$$

$$\dot{\Phi} = p + \dot{\psi} \sin \theta$$
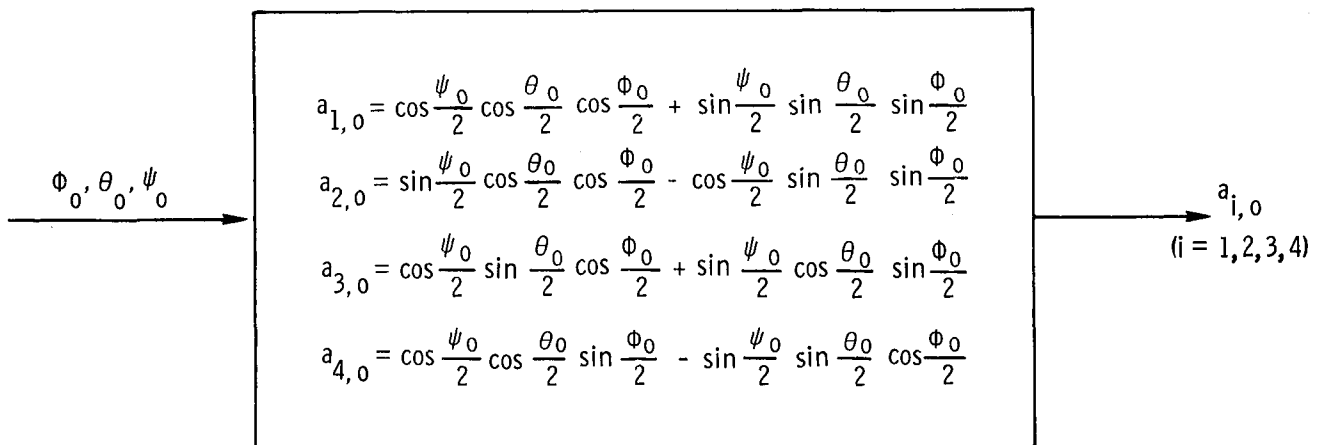
(b) Gimbal angle rates.

Quaternion rate differential equations

$$\dot{a}_1 = (-a_4 p - a_3 q - a_2 r)/2$$
$$\dot{a}_2 = (-a_3 p + a_4 q + a_1 r)/2$$
$$\dot{a}_3 = (a_2 p + a_1 q - a_4 r)/2$$
$$\dot{a}_4 = (a_1 p - a_2 q + a_3 r)/2$$

p
q
r

Elements of transformation matrix from wrist to hand

$$c_{11} = a_1^2 - a_2^2 - a_3^2 + a_4^2$$
$$c_{21} = 2(a_3 a_4 - a_1 a_2)$$
$$c_{31} = 2(a_1 a_3 + a_2 a_4)$$
$$c_{12} = 2(a_3 a_4 + a_1 a_2)$$
$$c_{22} = a_1^2 - a_2^2 + a_3^2 - a_4^2$$
$$c_{32} = 2(a_2 a_3 - a_1 a_4)$$
$$c_{13} = 2(a_2 a_4 - a_1 a_3)$$
$$c_{23} = 2(a_2 a_3 + a_4 a_1)$$
$$c_{33} = a_1^2 + a_2^2 - a_3^2 - a_4^2$$

Gimbal angle equations

$$\Phi = \tan^{-1}\left(\frac{c_{23}}{c_{33}}\right)$$

$$\psi = \tan^{-1}\left(\frac{c_{31} \sin \Phi - c_{21} \cos \Phi}{c_{22} \cos \Phi - c_{32} \sin \Phi}\right)$$

$$\theta = \tan^{-1}\left(\frac{-c_{13}}{c_{23} \sin \Phi + c_{33} \cos \Phi}\right)$$

Φ
ψ
θ

(c) Integration of quaternion rate equations to get gimbal angles.

Figure 1. Concluded.
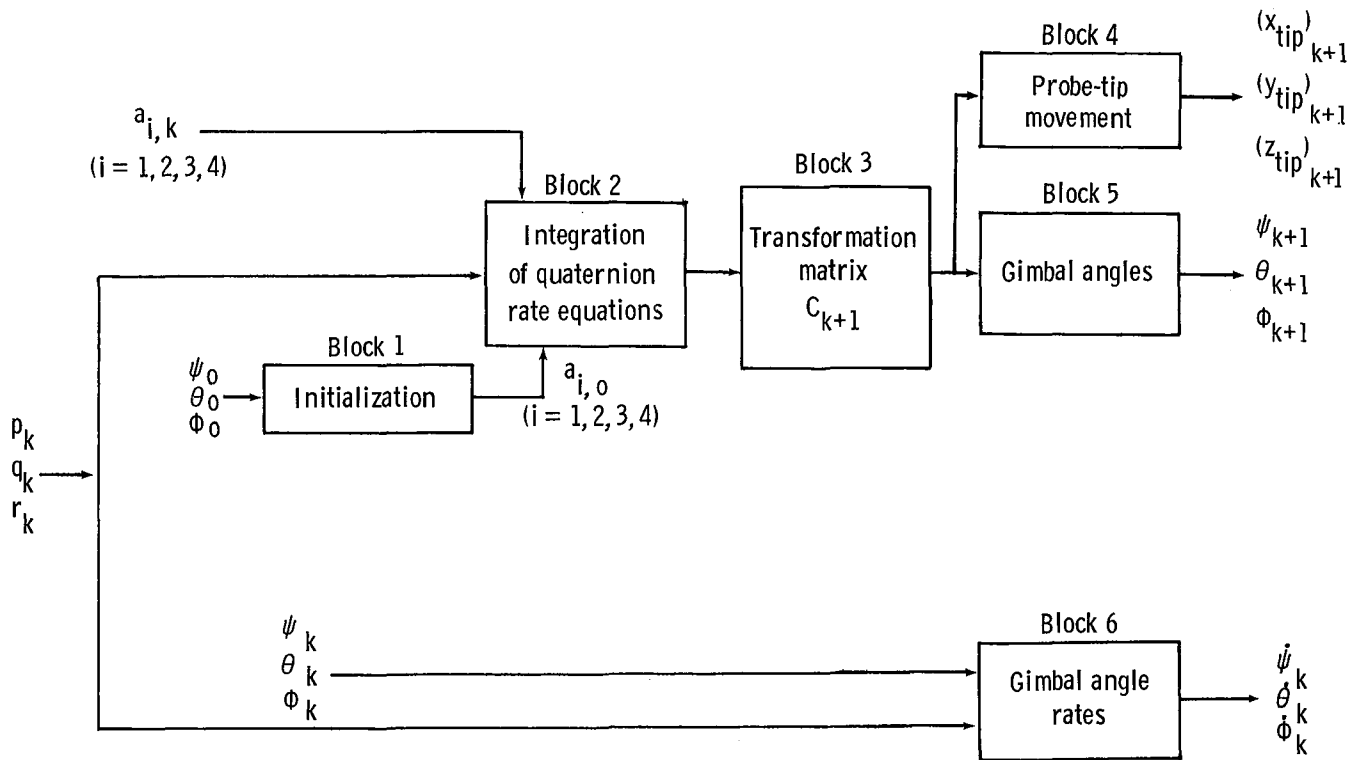
(a) Overview.

Gimbal angle to quaternion initialization
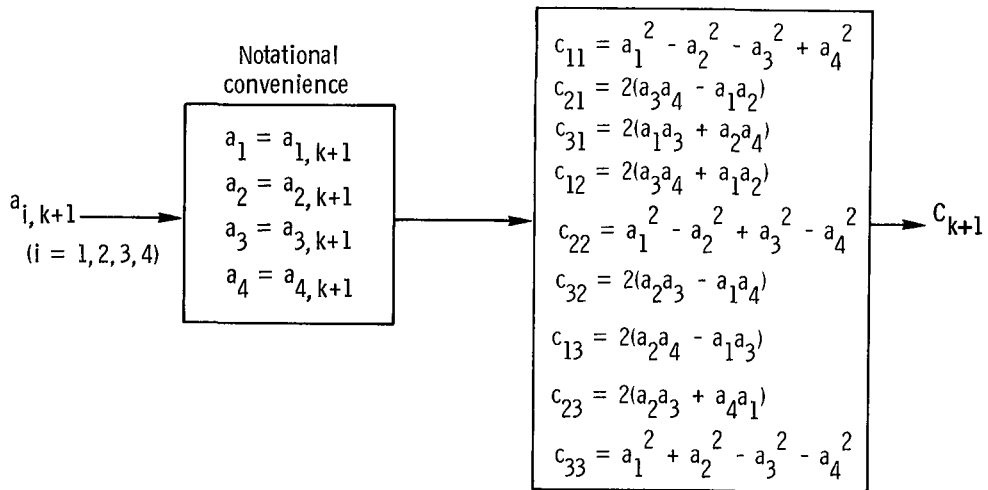
$$a_{1,0} = \cos\frac{\psi_0}{2}\cos\frac{\theta_0}{2}\cos\frac{\Phi_0}{2} + \sin\frac{\psi_0}{2}\sin\frac{\theta_0}{2}\sin\frac{\Phi_0}{2}$$

$$a_{2,0} = \sin\frac{\psi_0}{2}\cos\frac{\theta_0}{2}\cos\frac{\Phi_0}{2} - \cos\frac{\psi_0}{2}\sin\frac{\theta_0}{2}\sin\frac{\Phi_0}{2}$$

$$a_{3,0} = \cos\frac{\psi_0}{2}\sin\frac{\theta_0}{2}\cos\frac{\Phi_0}{2} + \sin\frac{\psi_0}{2}\cos\frac{\theta_0}{2}\sin\frac{\Phi_0}{2}$$

$$a_{4,0} = \cos\frac{\psi_0}{2}\cos\frac{\theta_0}{2}\sin\frac{\Phi_0}{2} - \sin\frac{\psi_0}{2}\sin\frac{\theta_0}{2}\cos\frac{\Phi_0}{2}$$

$\Phi_0, \theta_0, \psi_0 \longrightarrow$

$\longrightarrow a_{i,0}$
$(i = 1, 2, 3, 4)$

(b) Block 1 (initialization).

Figure 2. Block diagram of discrete equations for three-gimbal robot wrist.

Block 2 diagram:

$$\omega_k = \sqrt{p_k^2 + q_k^2 + r_k^2}$$

$$p_k = (\omega_k h)/2$$

$$C_1 = \cos p_k$$

$$C_2' = (\sin p_k)/\omega_k$$

$$H = C_1$$

$$G = -C_2' r_k$$

$$J = C_2' q_k$$

$$K = C_2' p_k$$

Inputs: p_k, q_k, r_k

$a_{i,k}$ $(i = 1, 2, 3, 4)$

Updated quaternions

$$a_{1,k+1} = Ha_{1,k} + Ga_{2,k} - Ja_{3,k} - Ka_{4,k}$$

$$a_{2,k+1} = -Ga_{1,k} + Ha_{2,k} - Ka_{3,k} + Ja_{4,k}$$

$$a_{3,k+1} = Ja_{1,k} + Ka_{2,k} + Ha_{3,k} + Ga_{4,k}$$

$$a_{4,k+1} = Ka_{1,k} - Ja_{2,k} - Ga_{3,k} + Ha_{4,k}$$

$a_{i,0}$ $(i = 1, 2, 3, 4)$

Normalization

$$N^2 = \sum_{i=1}^{i=4} (a_{i,k+1})^2$$

$$a_{i,k+1} = a_{i,k+1}/N$$

$$(i = 1, 2, 3, 4)$$

$a_{i,k+1}$ $(i = 1, 2, 3, 4)$
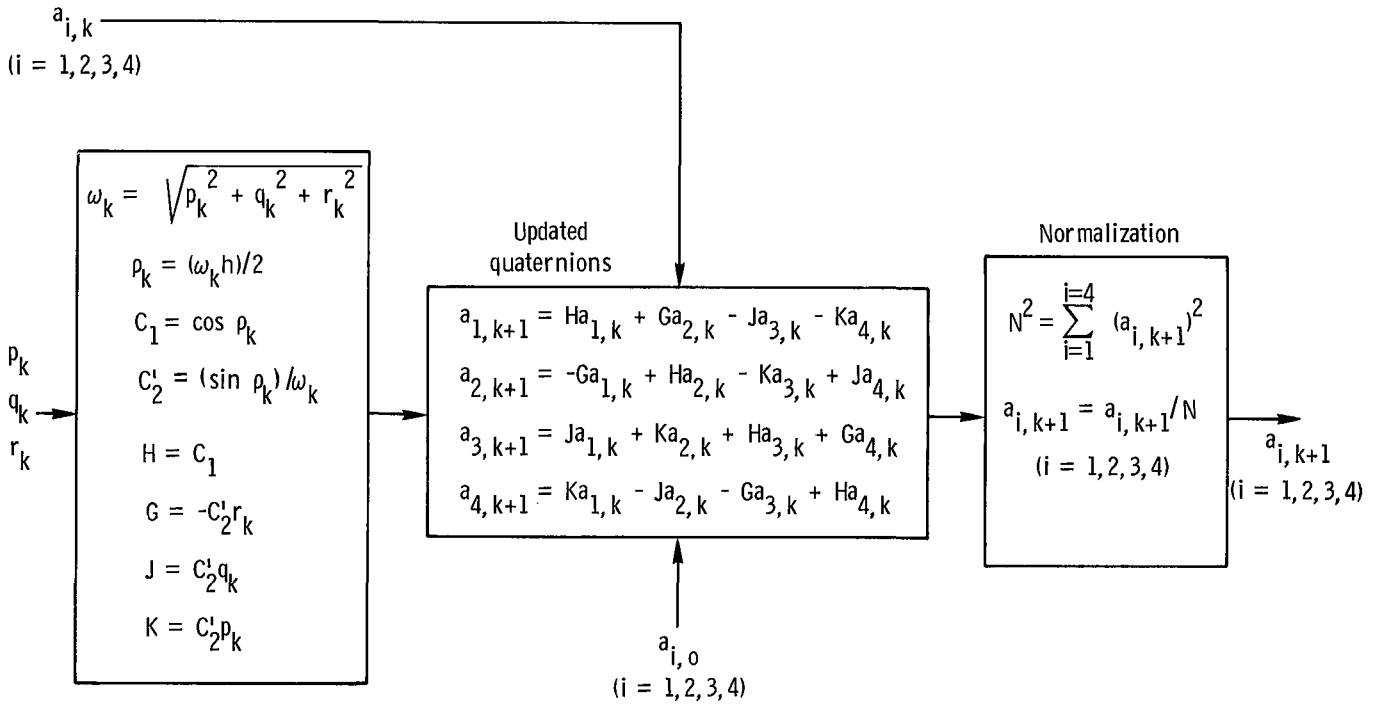
(c) Block 2 (integration of quaternion rate equations).

Block 3 diagram:

$a_{i,k+1}$ $(i = 1, 2, 3, 4)$

Notational convenience

$$a_1 = a_{1,k+1}$$
$$a_2 = a_{2,k+1}$$
$$a_3 = a_{3,k+1}$$
$$a_4 = a_{4,k+1}$$

$$c_{11} = a_1^2 - a_2^2 - a_3^2 + a_4^2$$

$$c_{21} = 2(a_3 a_4 - a_1 a_2)$$

$$c_{31} = 2(a_1 a_3 + a_2 a_4)$$

$$c_{12} = 2(a_3 a_4 + a_1 a_2)$$

$$c_{22} = a_1^2 - a_2^2 + a_3^2 - a_4^2$$

$$c_{32} = 2(a_2 a_3 - a_1 a_4)$$

$$c_{13} = 2(a_2 a_4 - a_1 a_3)$$

$$c_{23} = 2(a_2 a_3 + a_4 a_1)$$

$$c_{33} = a_1^2 + a_2^2 - a_3^2 - a_4^2$$

C_{k+1}

(d) Block 3 (transformation matrix C_{k+1}).

Figure 2. Continued.

C_{k+1} →

$$C_{k+1}^T \begin{pmatrix} l_x \\ l_y \\ l_z \end{pmatrix} = C_{k+1}^T \begin{pmatrix} 6 \text{ in.} \\ 0 \\ 0 \end{pmatrix} = 6 \begin{pmatrix} c_{11} \\ c_{12} \\ c_{13} \end{pmatrix}_{k+1}$$

→ $\begin{pmatrix} x_{tip} \\ y_{tip} \\ z_{tip} \end{pmatrix}_{k+1}$

Probe-tip
coordinates in
moving robot-
hand axis
system (X, Y, Z)

Probe-tip position
projected onto robot-
forearm axis system
(X_F, Y_F, Z_F)
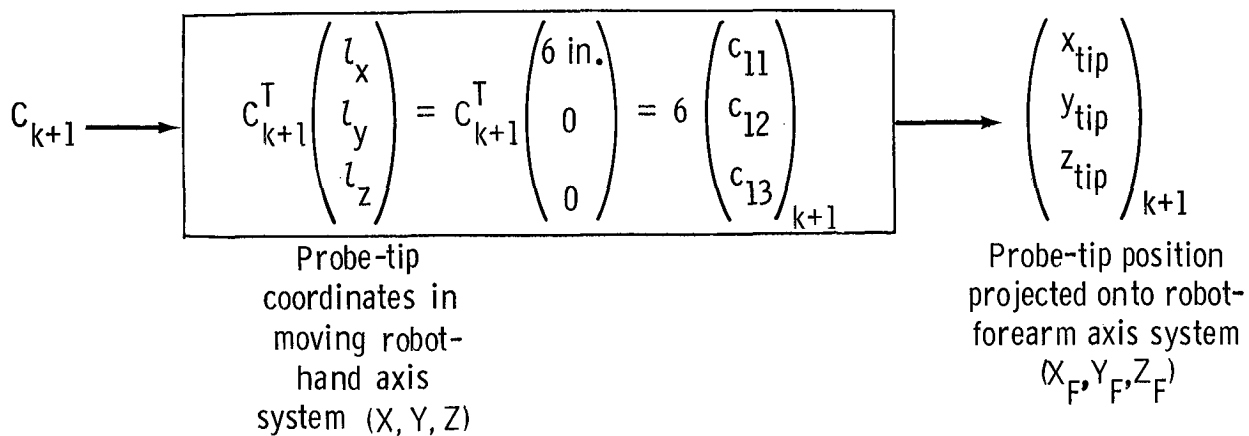
(e) Block 4 (probe-tip movement).

C_{k+1} →

$$\phi_{k+1} = \tan^{-1}\left(\frac{c_{23}}{c_{33}}\right)_{k+1}$$

$$\psi_{k+1} = \tan^{-1}\left(\frac{c_{31} \sin \phi - c_{21} \cos \phi}{c_{22} \cos \phi - c_{32} \sin \phi}\right)_{k+1}$$

$$\theta_{k+1} = \tan^{-1}\left(\frac{-c_{13}}{c_{23} \sin \phi + c_{33} \cos \phi}\right)_{k+1}$$

→ ϕ_{k+1}
ψ_{k+1}
θ_{k+1}

(f) Block 5 (gimbal angles).

ψ_k
θ_k →
ϕ_k

p_k
q_k →
r_k

$$\dot{\psi}_k = \left(\frac{r \cos \phi + q \sin \phi}{\cos \theta}\right)_k$$

$$\dot{\theta}_k = (q \cos \phi - r \sin \phi)_k$$

$$\dot{\phi}_k = (p + \dot{\psi} \sin \theta)_k$$

→ $\dot{\psi}_k$
$\dot{\theta}_k$
$\dot{\phi}_k$
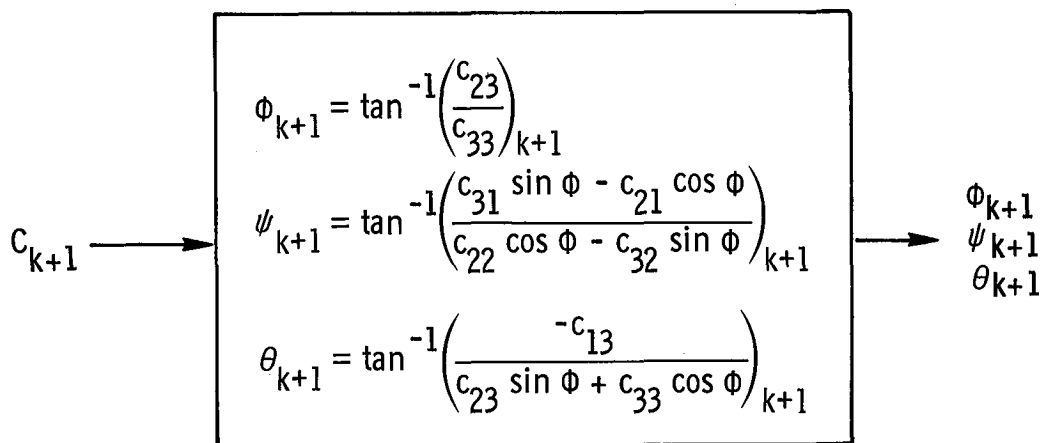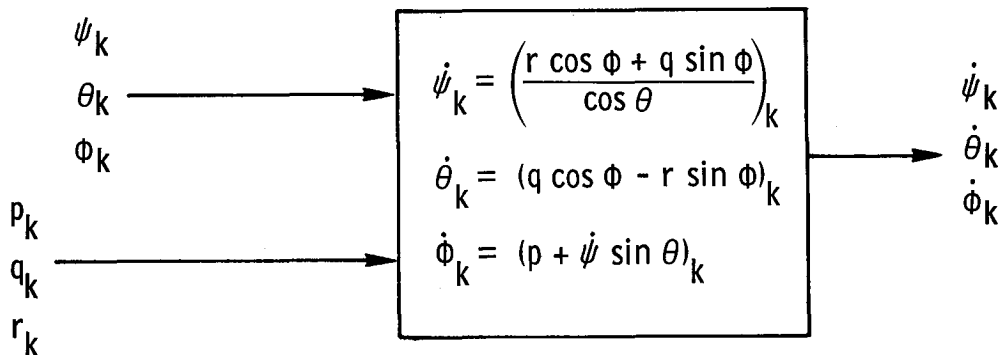
(g) Block 6 (gimbal angle rates).

Figure 2. Concluded.
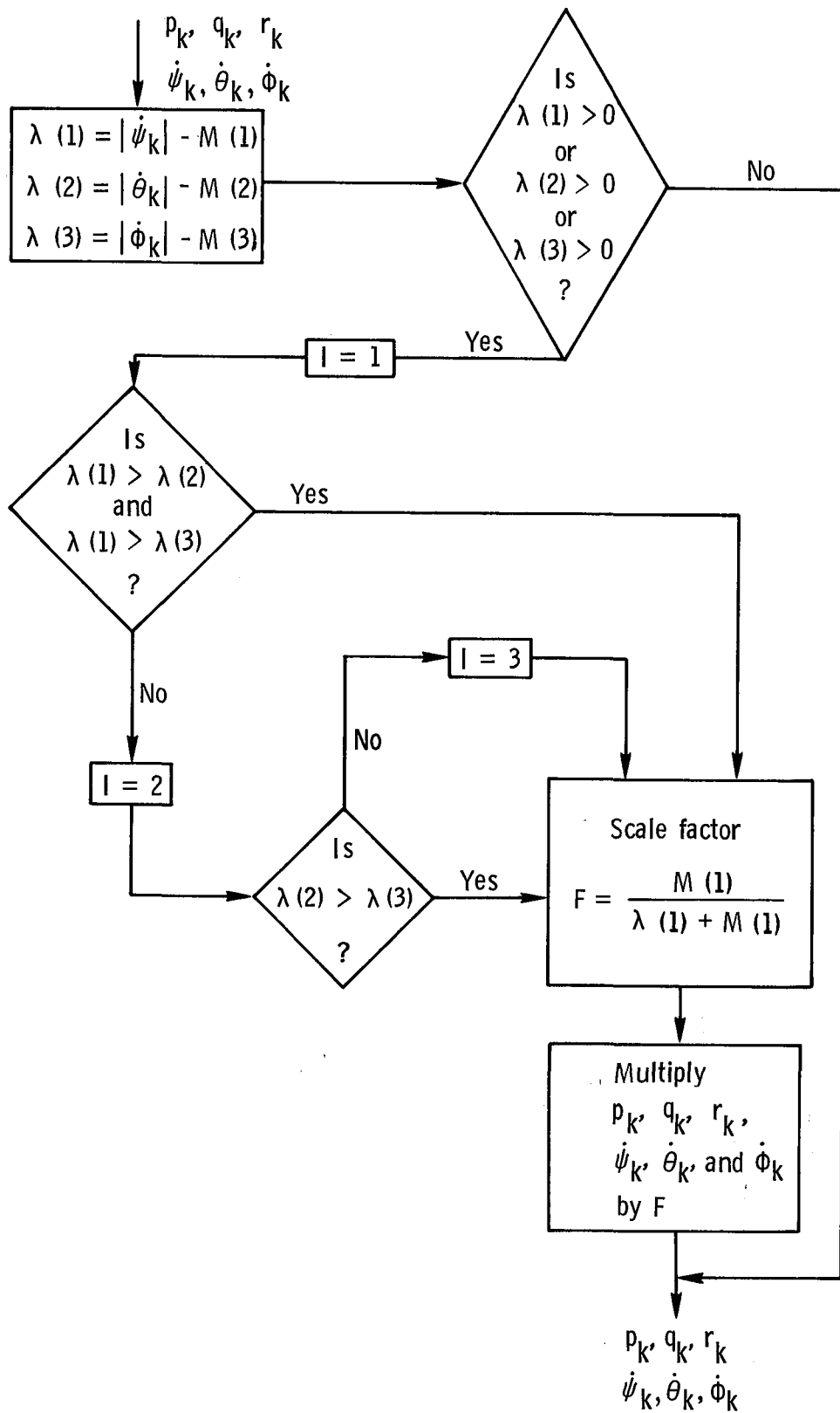
(a) Away from singularity.

Figure 3. Scaling procedure.
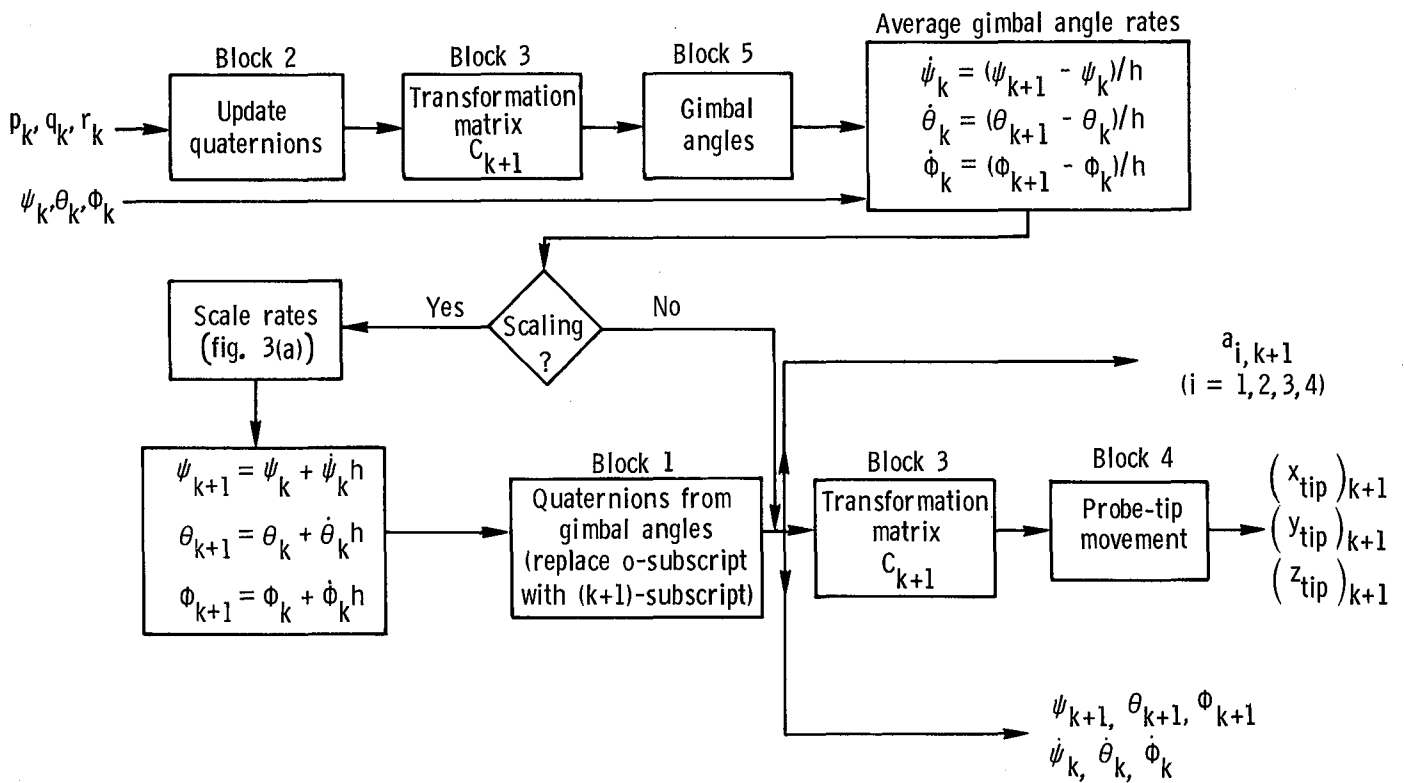
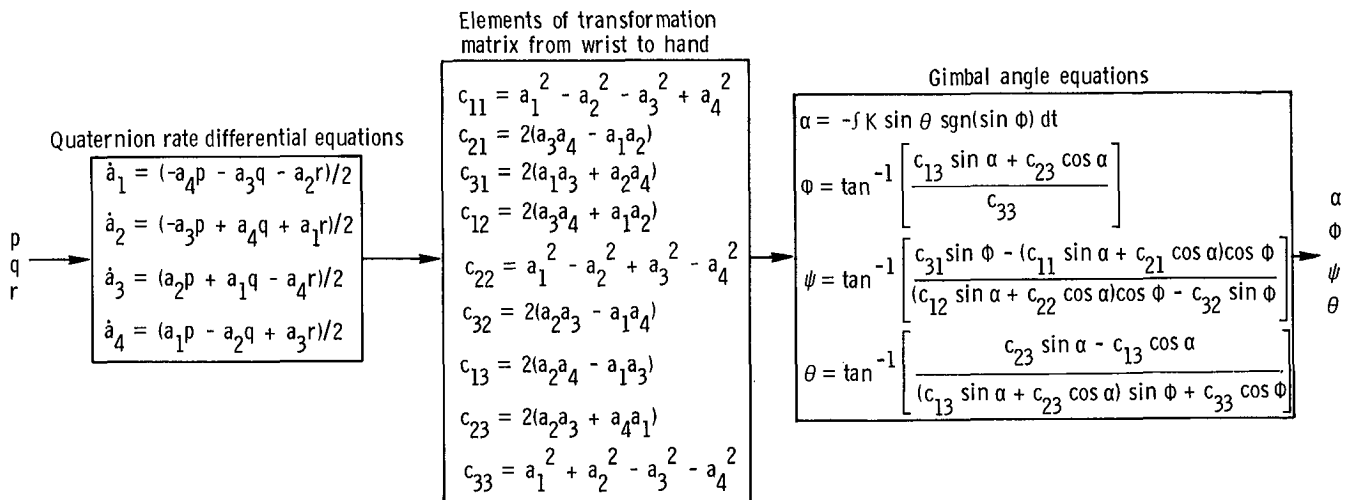(b) At or near singularity.

Figure 3. Concluded.
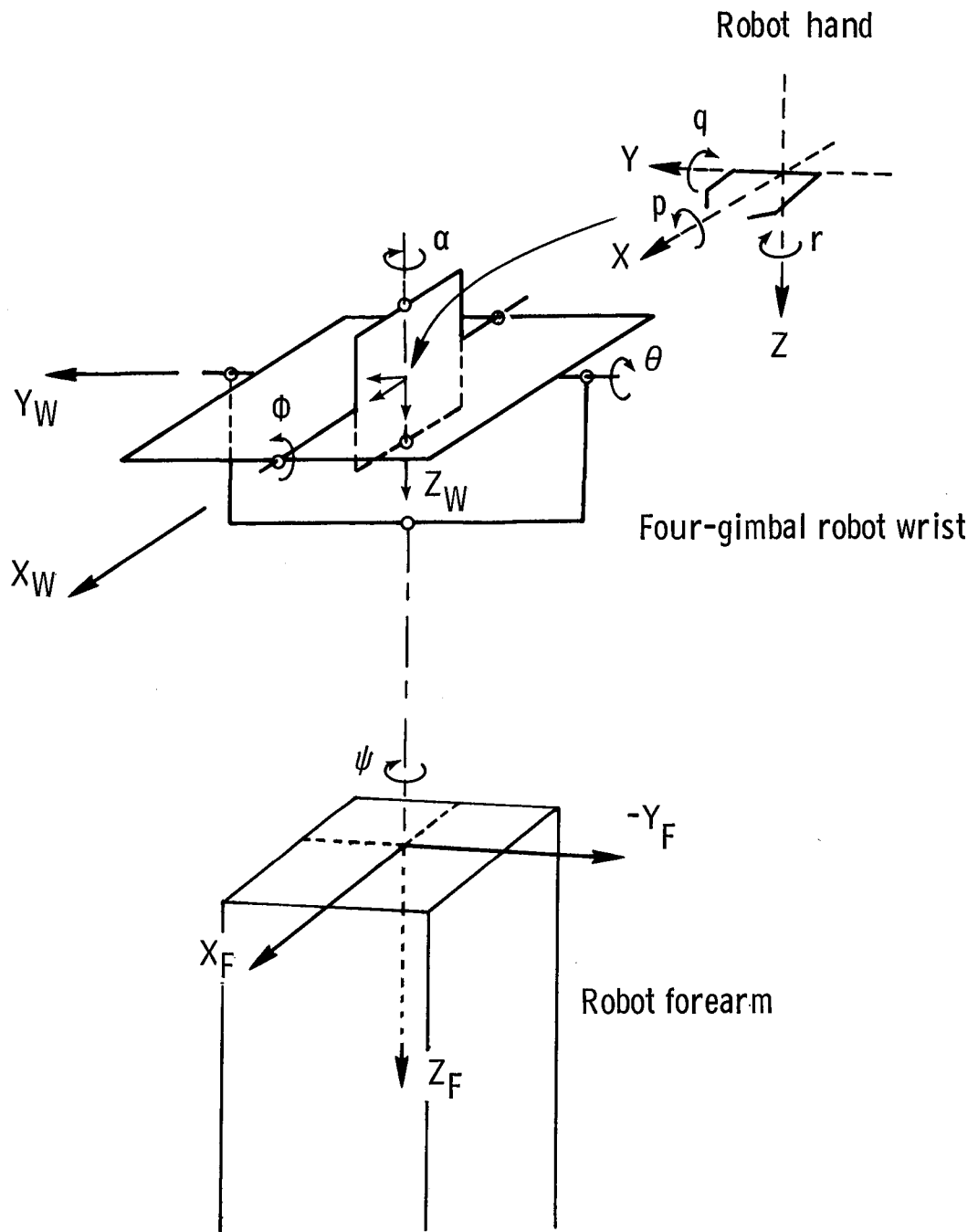
(a) Axis systems.
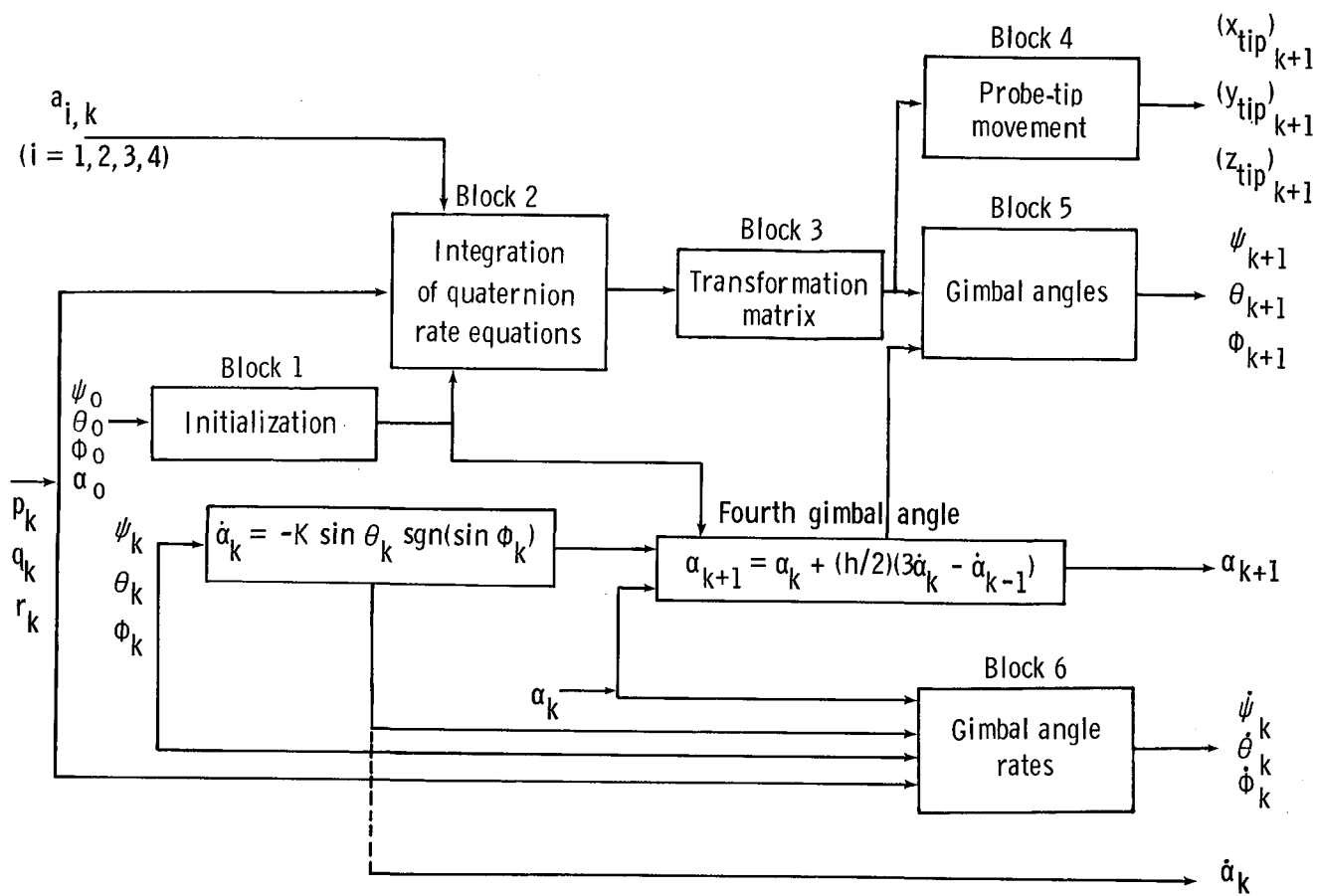
Figure 4. Robot hand with four-gimbal robot wrist.

$$\dot{\alpha} = -K \sin \theta \, \mathrm{sgn}(\sin \phi)$$

$$\dot{\psi} = \frac{(p \sin \alpha + q \cos \alpha)\sin \phi + (r - \dot{\alpha})\cos \phi}{\cos \theta}$$

$$\dot{\theta} = (p \sin \alpha + q \cos \alpha)\cos \phi - (r - \dot{\alpha})\sin \phi$$

$$\dot{\phi} = (p \cos \alpha - q \sin \alpha) + \dot{\psi} \sin \theta$$

(b) Gimbal angle rates.

Elements of transformation matrix from wrist to hand

Quaternion rate differential equations

$$\dot{a}_1 = (-a_4 p - a_3 q - a_2 r)/2$$
$$\dot{a}_2 = (-a_3 p + a_4 q + a_1 r)/2$$
$$\dot{a}_3 = (a_2 p + a_1 q - a_4 r)/2$$
$$\dot{a}_4 = (a_1 p - a_2 q + a_3 r)/2$$

$$c_{11} = a_1^2 - a_2^2 - a_3^2 + a_4^2$$
$$c_{21} = 2(a_3 a_4 - a_1 a_2)$$
$$c_{31} = 2(a_1 a_3 + a_2 a_4)$$
$$c_{12} = 2(a_3 a_4 + a_1 a_2)$$
$$c_{22} = a_1^2 - a_2^2 + a_3^2 - a_4^2$$
$$c_{32} = 2(a_2 a_3 - a_1 a_4)$$
$$c_{13} = 2(a_2 a_4 - a_1 a_3)$$
$$c_{23} = 2(a_2 a_3 + a_4 a_1)$$
$$c_{33} = a_1^2 + a_2^2 - a_3^2 - a_4^2$$

Gimbal angle equations

$$\alpha = -\int K \sin \theta \, \mathrm{sgn}(\sin \phi) \, dt$$

$$\phi = \tan^{-1}\left[\frac{c_{13} \sin \alpha + c_{23} \cos \alpha}{c_{33}}\right]$$

$$\psi = \tan^{-1}\left[\frac{c_{31} \sin \phi - (c_{11} \sin \alpha + c_{21} \cos \alpha)\cos \phi}{(c_{12} \sin \alpha + c_{22} \cos \alpha)\cos \phi - c_{32} \sin \phi}\right]$$

$$\theta = \tan^{-1}\left[\frac{c_{23} \sin \alpha - c_{13} \cos \alpha}{(c_{13} \sin \alpha + c_{23} \cos \alpha) \sin \phi + c_{33} \cos \phi}\right]$$

p
q
r

α
ϕ
ψ
θ

(c) Integration of quaternion rate equations to get gimbal angles.

Figure 4. Concluded.

(a) Overview.

$$\Phi_{k+1} = \tan^{-1}\left[\frac{(c_{13}\sin\alpha + c_{23}\cos\alpha)}{c_{33}}\right]_{k+1}$$

$$\psi_{k+1} = \tan^{-1}\left[\frac{c_{31}\sin\Phi - (c_{11}\sin\alpha + c_{21}\cos\alpha)\cos\Phi}{(c_{12}\sin\alpha + c_{22}\cos\alpha)\cos\Phi - c_{32}\sin\Phi}\right]_{k+1}$$

$$\theta_{k+1} = \tan^{-1}\left[\frac{c_{23}\sin\alpha - c_{13}\cos\alpha}{(c_{13}\sin\alpha + c_{23}\cos\alpha)\sin\Phi + c_{33}\cos\Phi}\right]_{k+1}$$
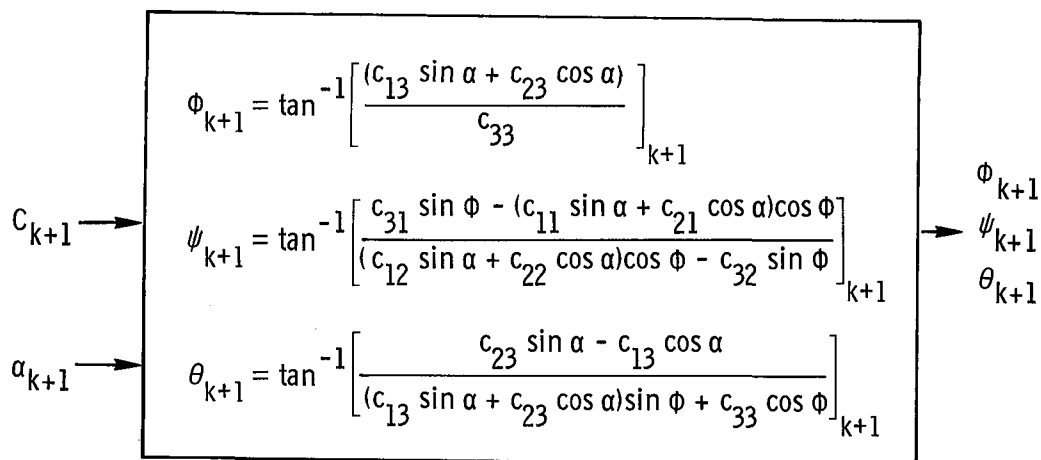
(b) Block 5 (gimbal angles).

Figure 5. Discrete calculations for four-gimbal robot wrist.

$$b_{1,0} = \cos\frac{\psi_0}{2}\cos\frac{\theta_0}{2}\cos\frac{\Phi_0}{2} + \sin\frac{\psi_0}{2}\sin\frac{\theta_0}{2}\sin\frac{\Phi_0}{2}$$

$$b_{2,0} = \sin\frac{\psi_0}{2}\cos\frac{\theta_0}{2}\cos\frac{\Phi_0}{2} - \cos\frac{\psi_0}{2}\sin\frac{\theta_0}{2}\sin\frac{\Phi_0}{2}$$

$$b_{3,0} = \cos\frac{\psi_0}{2}\sin\frac{\theta_0}{2}\cos\frac{\Phi_0}{2} + \sin\frac{\psi_0}{2}\cos\frac{\theta_0}{2}\sin\frac{\Phi_0}{2}$$

$$b_{4,0} = \cos\frac{\psi_0}{2}\cos\frac{\theta_0}{2}\sin\frac{\Phi_0}{2} - \sin\frac{\psi_0}{2}\sin\frac{\theta_0}{2}\cos\frac{\Phi_0}{2}$$

ψ_0
θ_0
Φ_0
α_0

$$a_{1,0} = b_{1,0}\cos\frac{\alpha_0}{2} - b_{2,0}\sin\frac{\alpha_0}{2}$$

$$a_{2,0} = b_{1,0}\sin\frac{\alpha_0}{2} + b_{2,0}\cos\frac{\alpha_0}{2}$$

$$a_{3,0} = b_{3,0}\cos\frac{\alpha_0}{2} - b_{4,0}\sin\frac{\alpha_0}{2}$$

$$a_{4,0} = b_{3,0}\sin\frac{\alpha_0}{2} + b_{4,0}\cos\frac{\alpha_0}{2}$$

$a_{i,0}$
$(i = 1, 2, 3, 4)$

Initialized past gimbal angle rate

$$\dot{\alpha}_0 = -K\sin\theta_0\,\text{sgn}(\sin\Phi_0)$$

$$\dot{\alpha}_{-1} = \dot{\alpha}_0$$

$\dot{\alpha}_{-1}$

(c) Block 1 (initialization).

α_k
$\dot{\alpha}_k$

ψ_k, θ_k, Φ_k

p_k, q_k, r_k

$$\dot{\psi}_k = \left[\frac{(p\sin\alpha + q\cos\alpha)\sin\Phi + (r - \dot{\alpha})\cos\Phi}{\cos\theta}\right]_k$$

$$\dot{\theta}_k = \left[(p\sin\alpha + q\cos\alpha)\cos\Phi - (r - \dot{\alpha})\sin\Phi\right]_k$$

$$\dot{\Phi}_k = \left[(p\cos\alpha - q\sin\alpha) + \dot{\psi}\sin\theta\right]_k$$

$\dot{\psi}_k$

$\dot{\theta}_k$

$\dot{\Phi}_k$
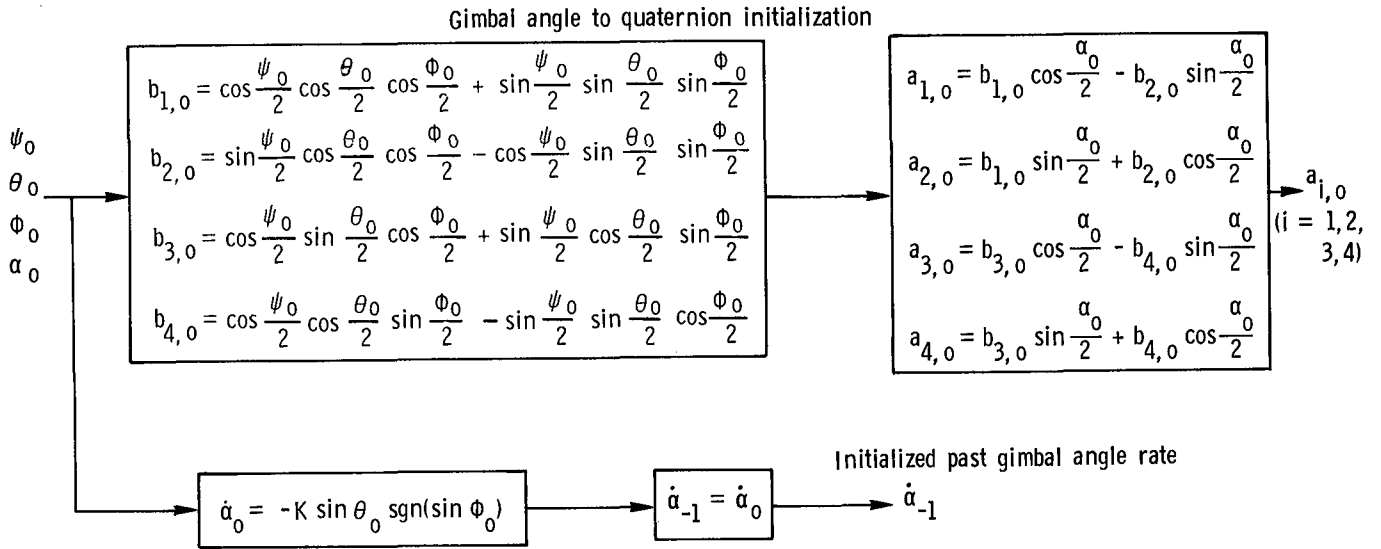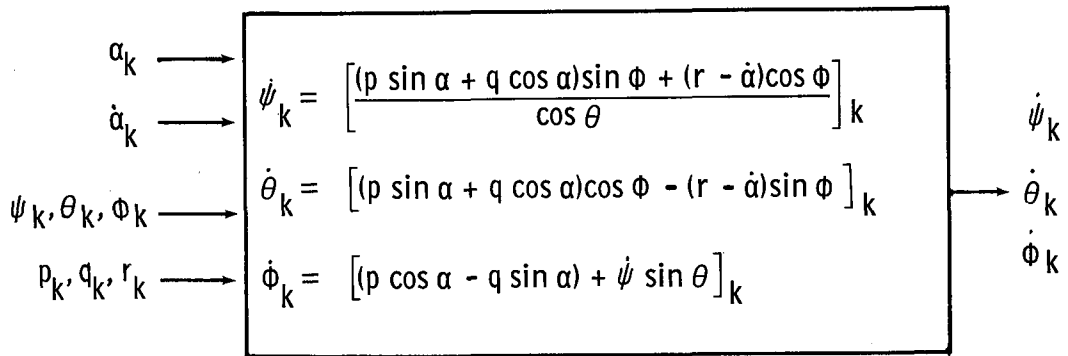
(d) Block 6 (gimbal angle rates).

Figure 5. Concluded.
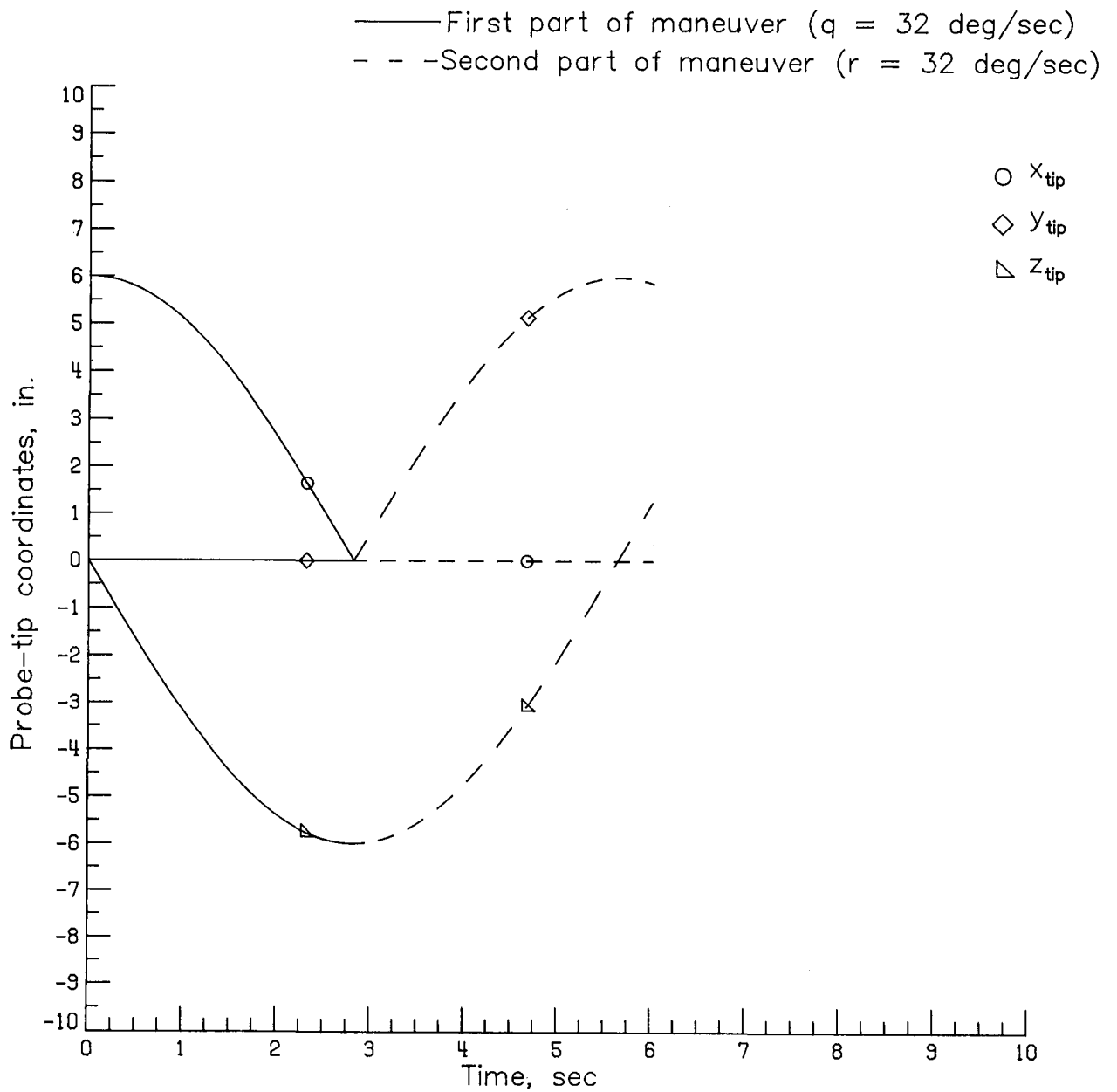
Figure 6. Ideal probe-tip movements for basic test maneuver.
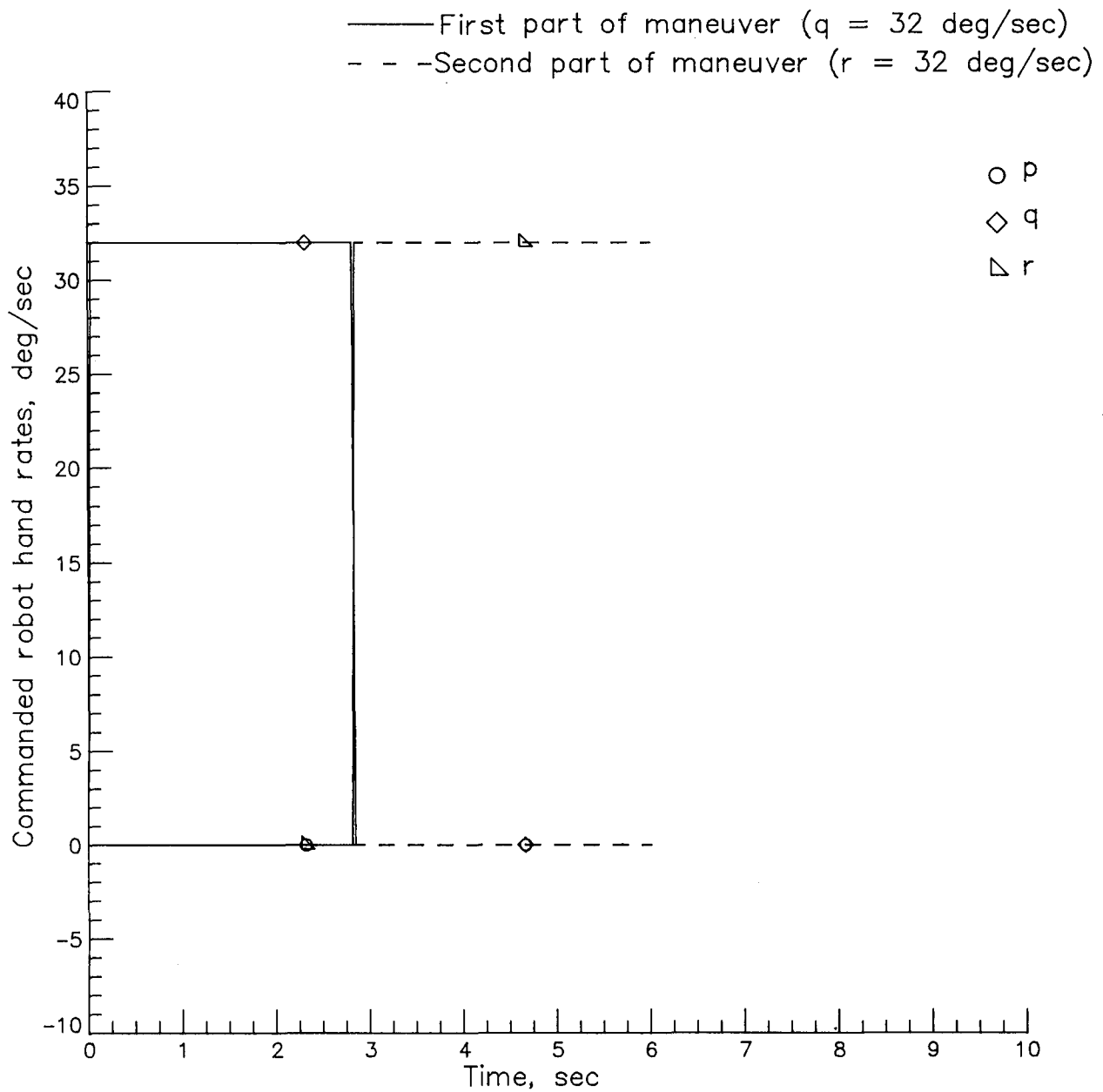
(a) Operator inputs.

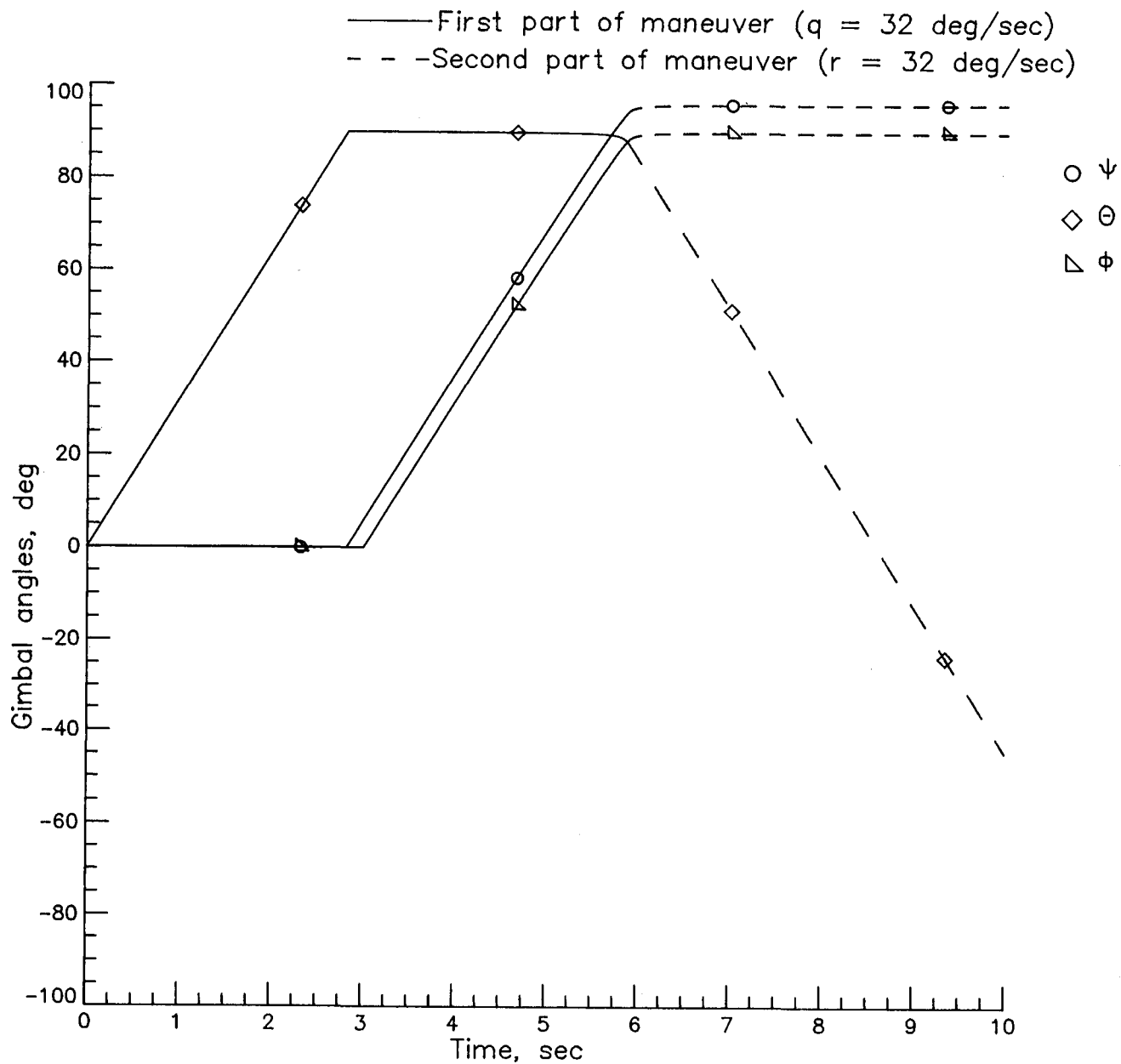Figure 7. Basic test maneuver with three-gimbal robot wrist with no scaling of gimbal angle rates.
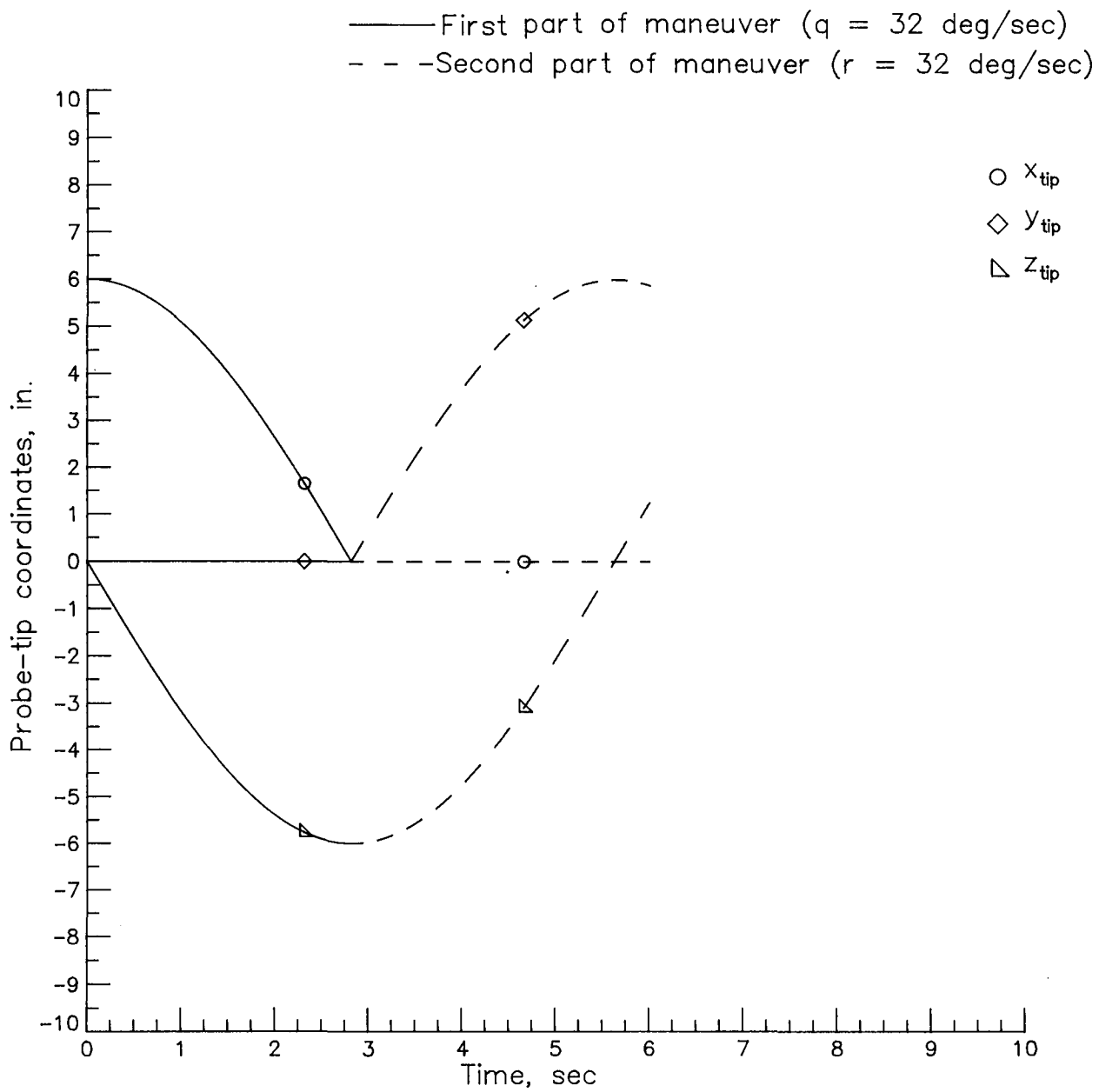
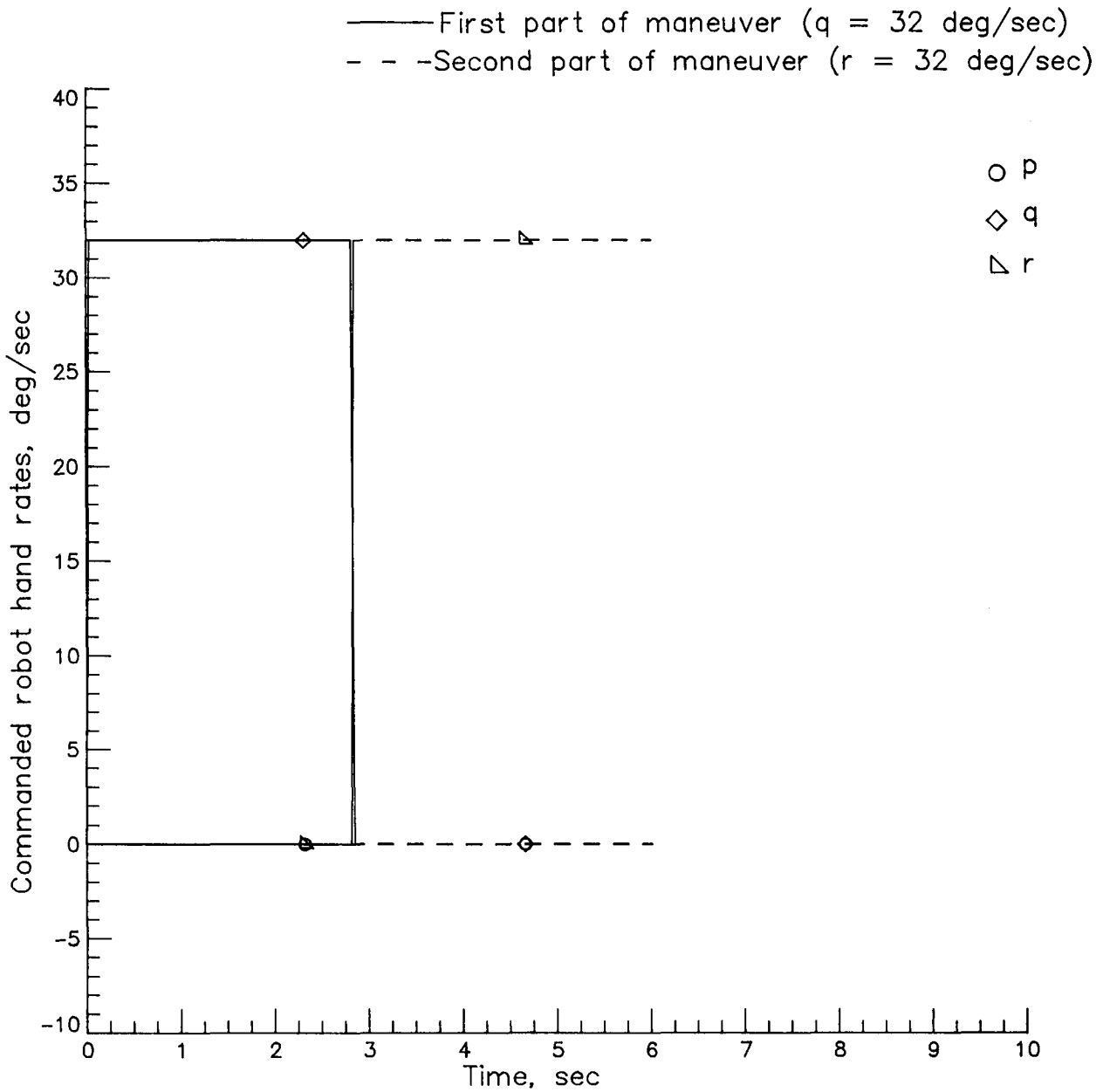(b) Probe-tip movement.

Figure 7. Continued.
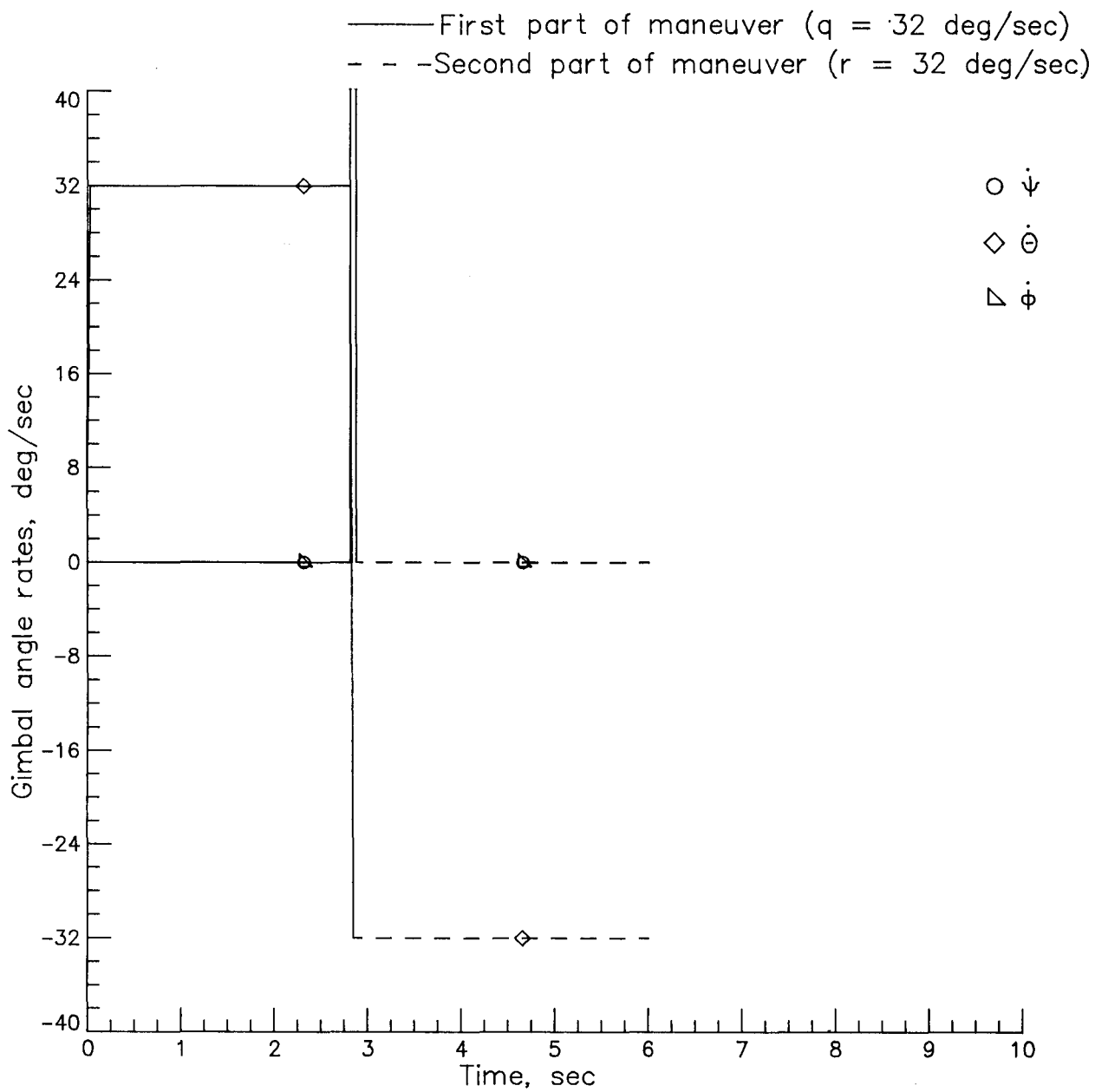
(c) Gimbal angle rates.

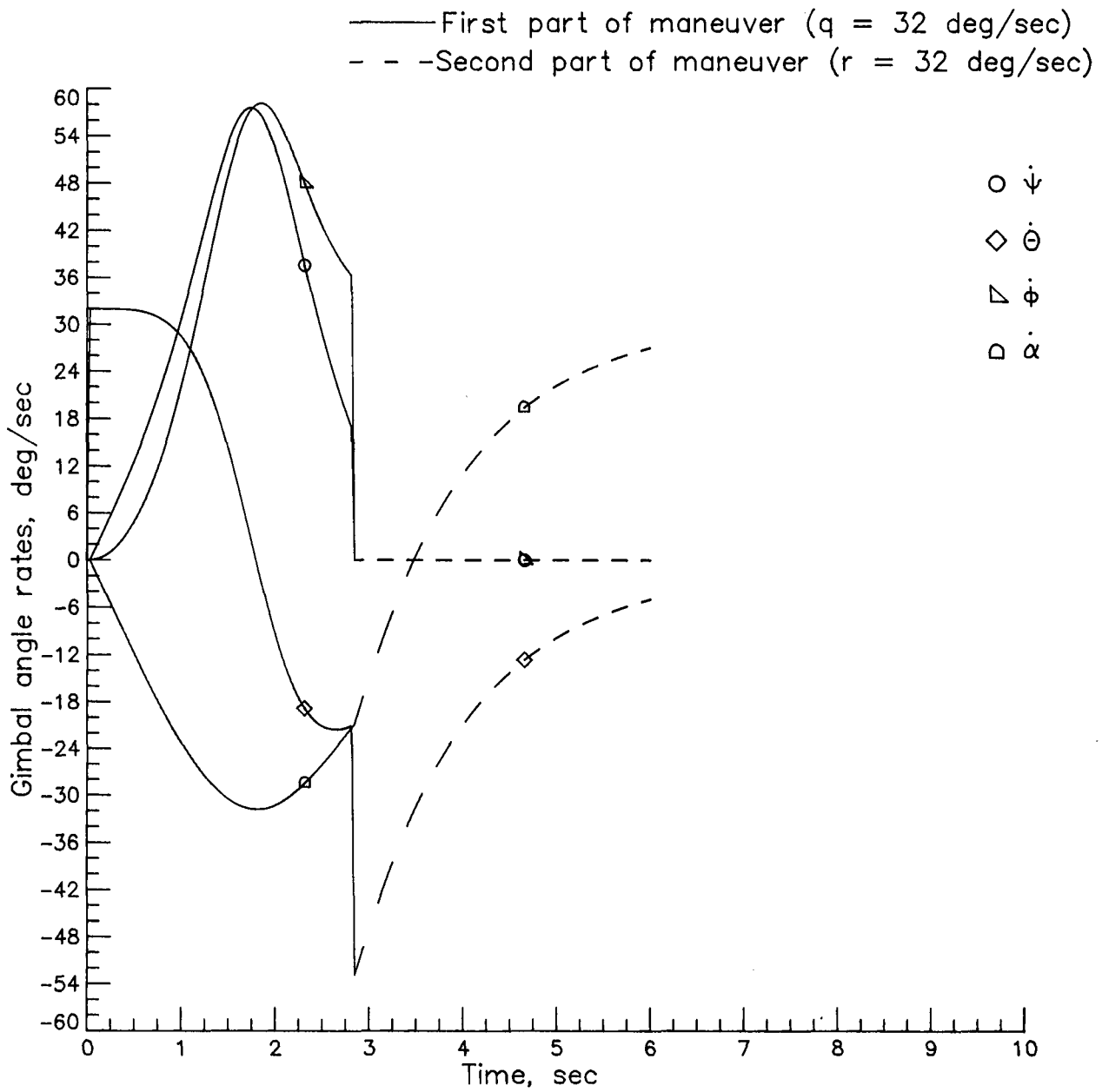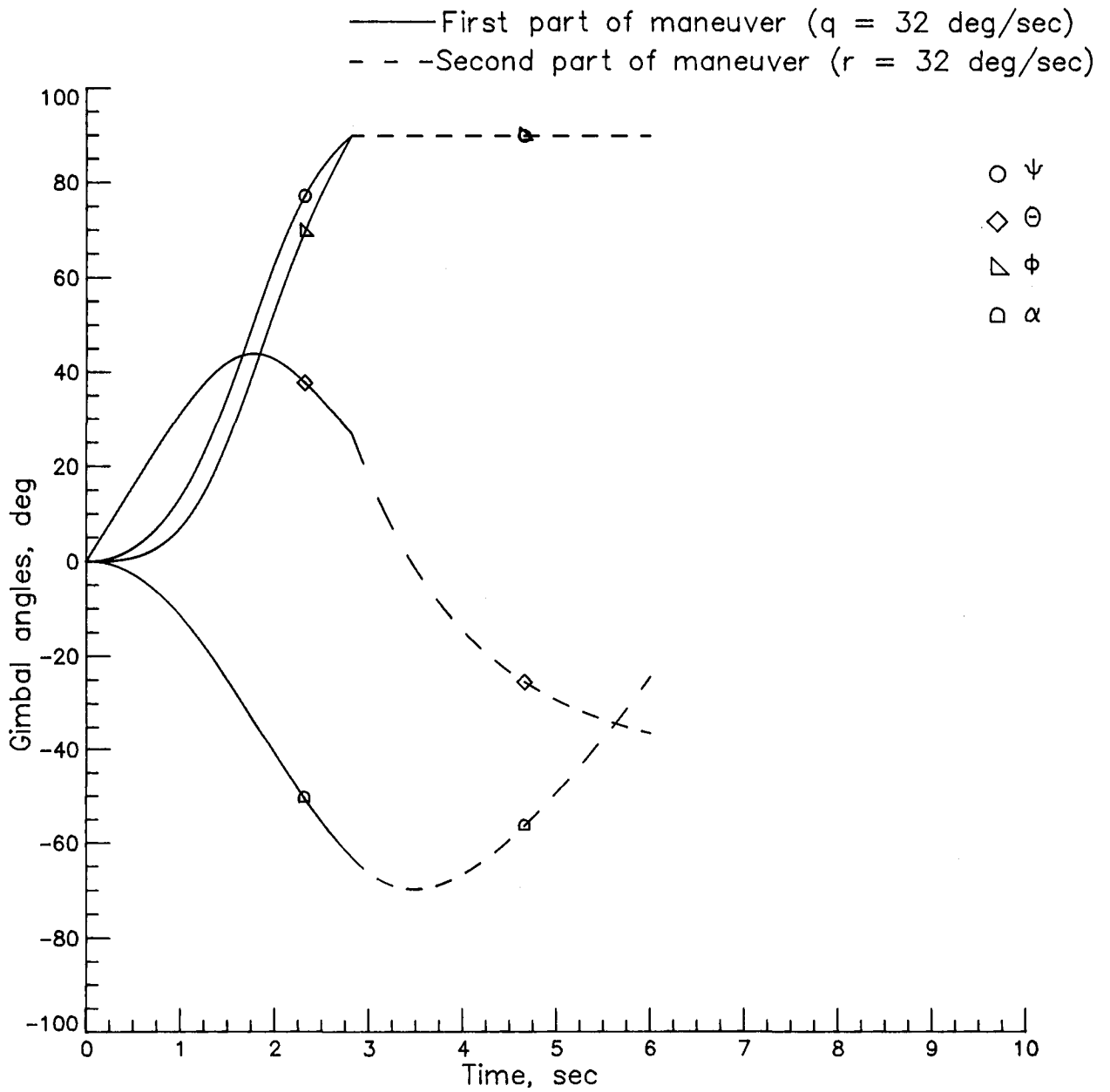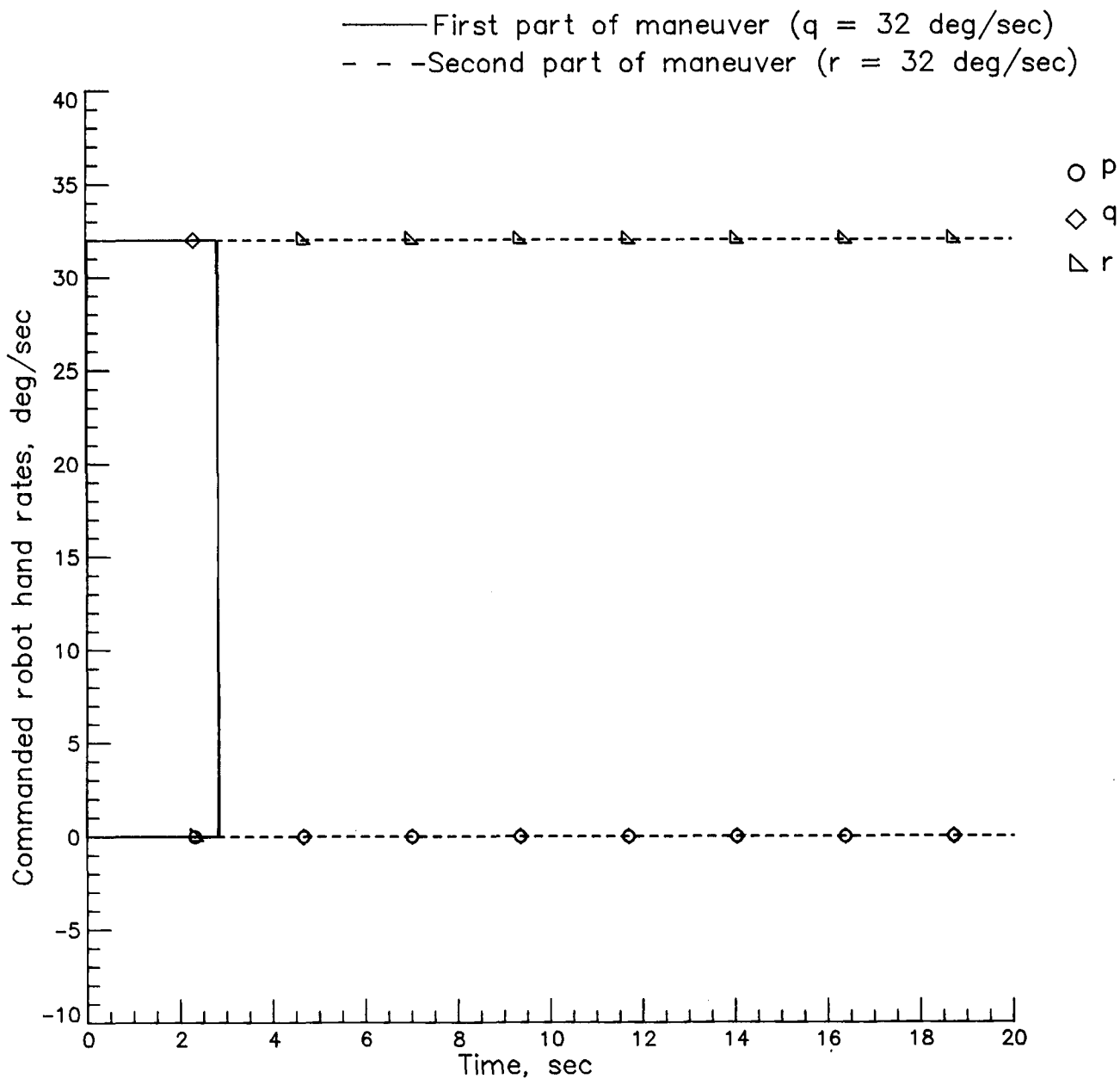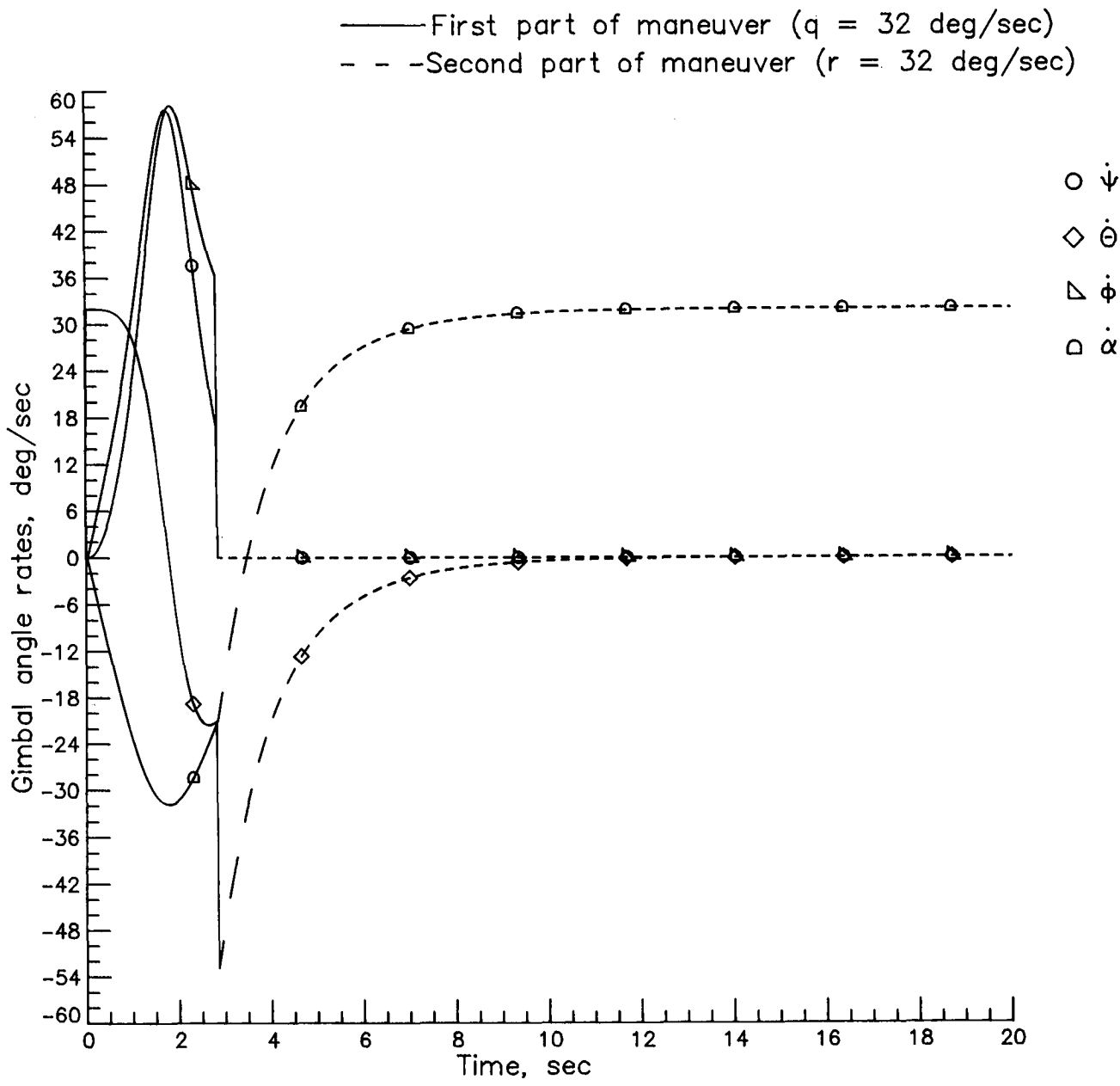Figure 7. Continued.
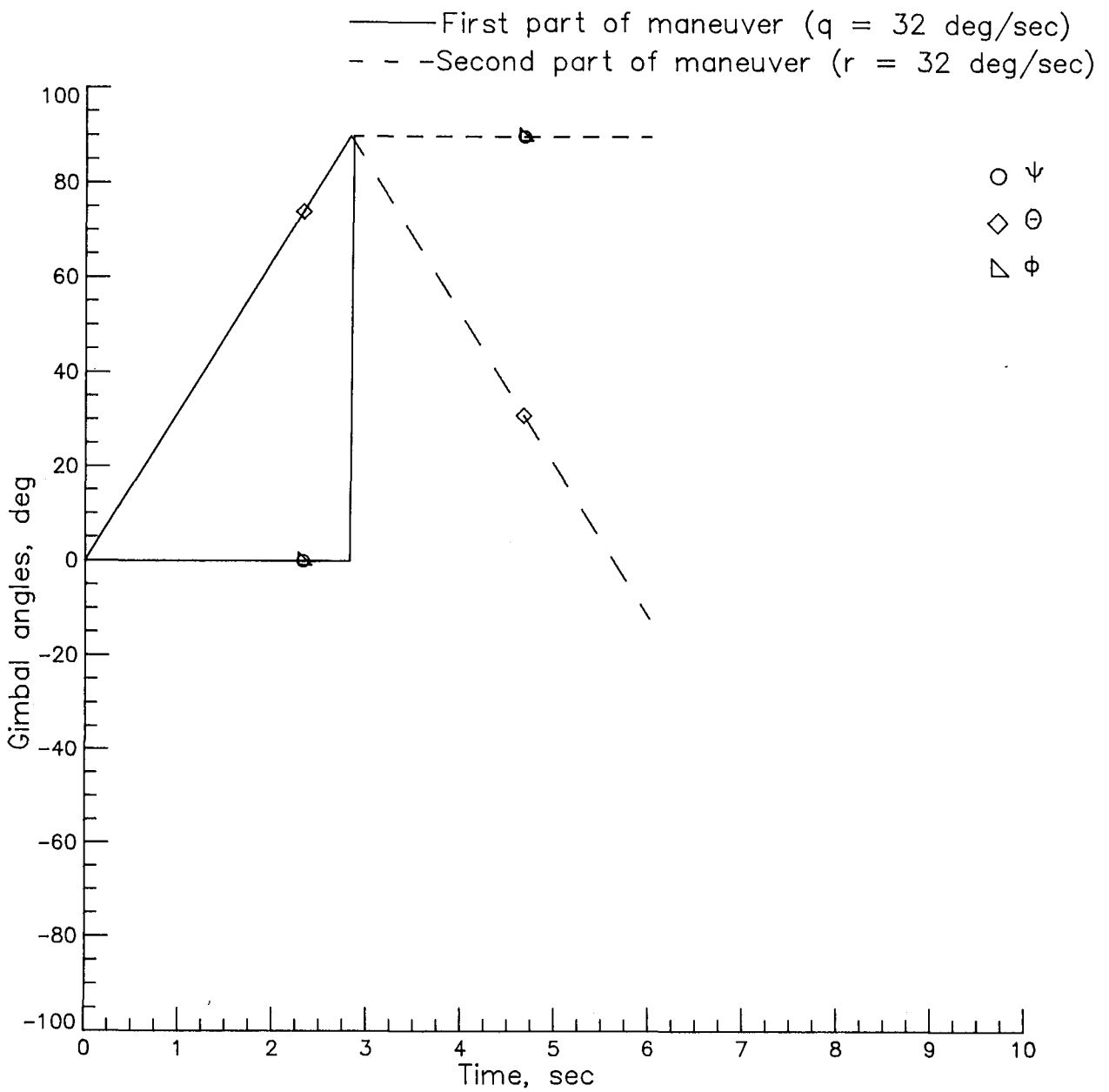
(d) Gimbal angles.

Figure 7. Concluded.
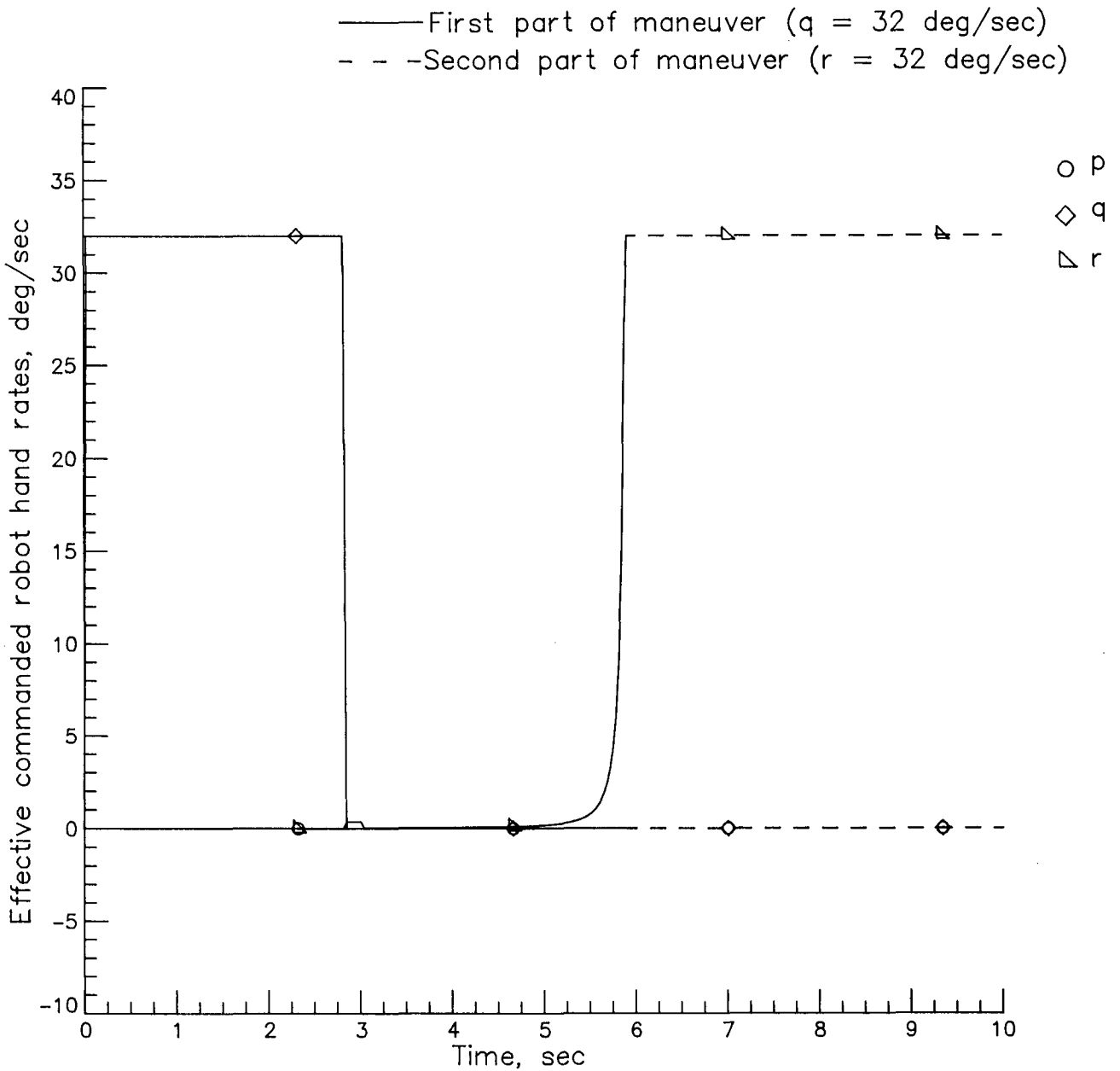
(a) Effective operator inputs.

Figure 8. Basic test maneuver with three-gimbal robot wrist with scaling of gimbal angle rates. (When required, rates are proportionally scaled so that no rate exceeds 32 deg/sec.)
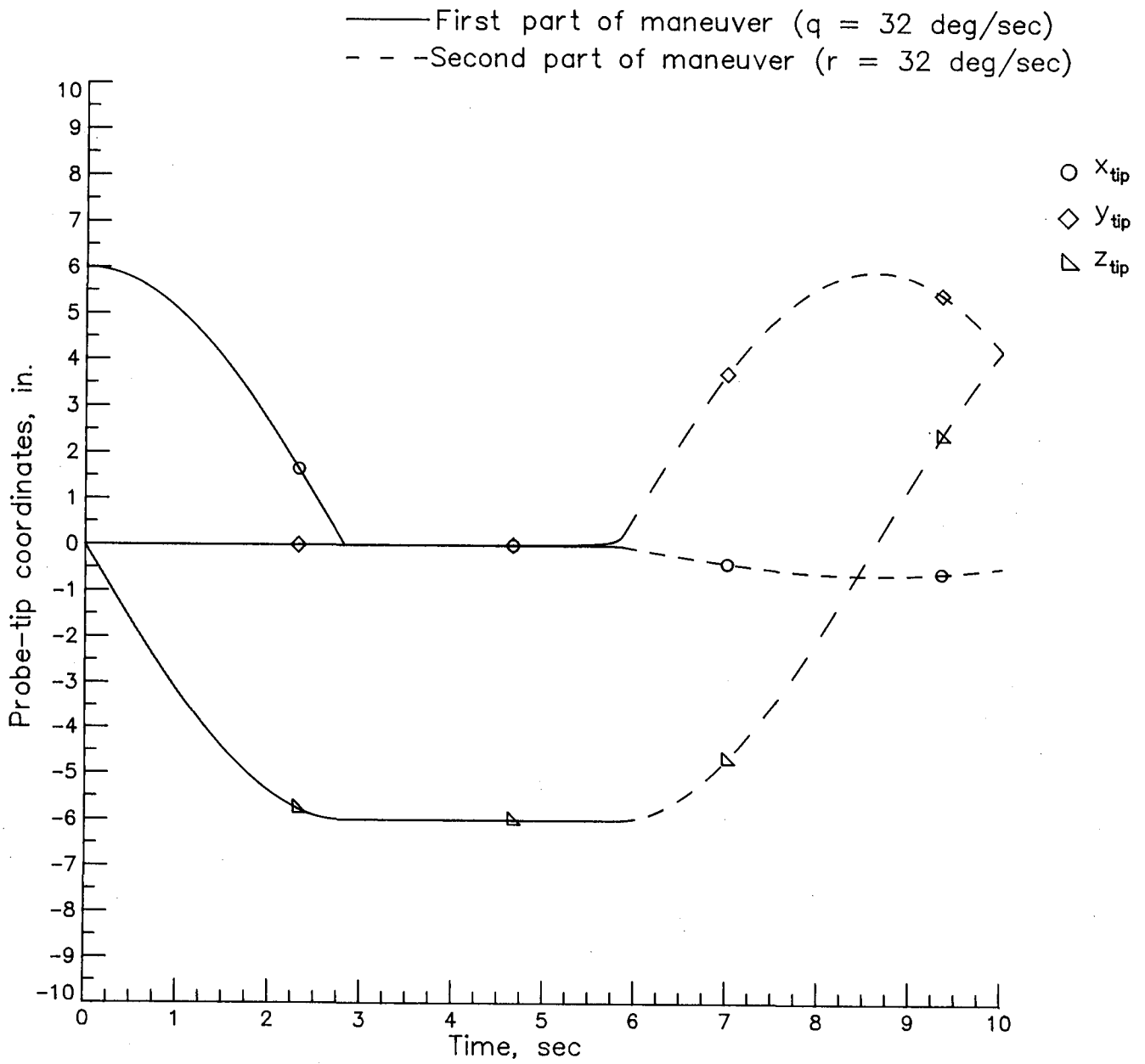
(b) Probe-tip movement.

Figure 8. Continued.
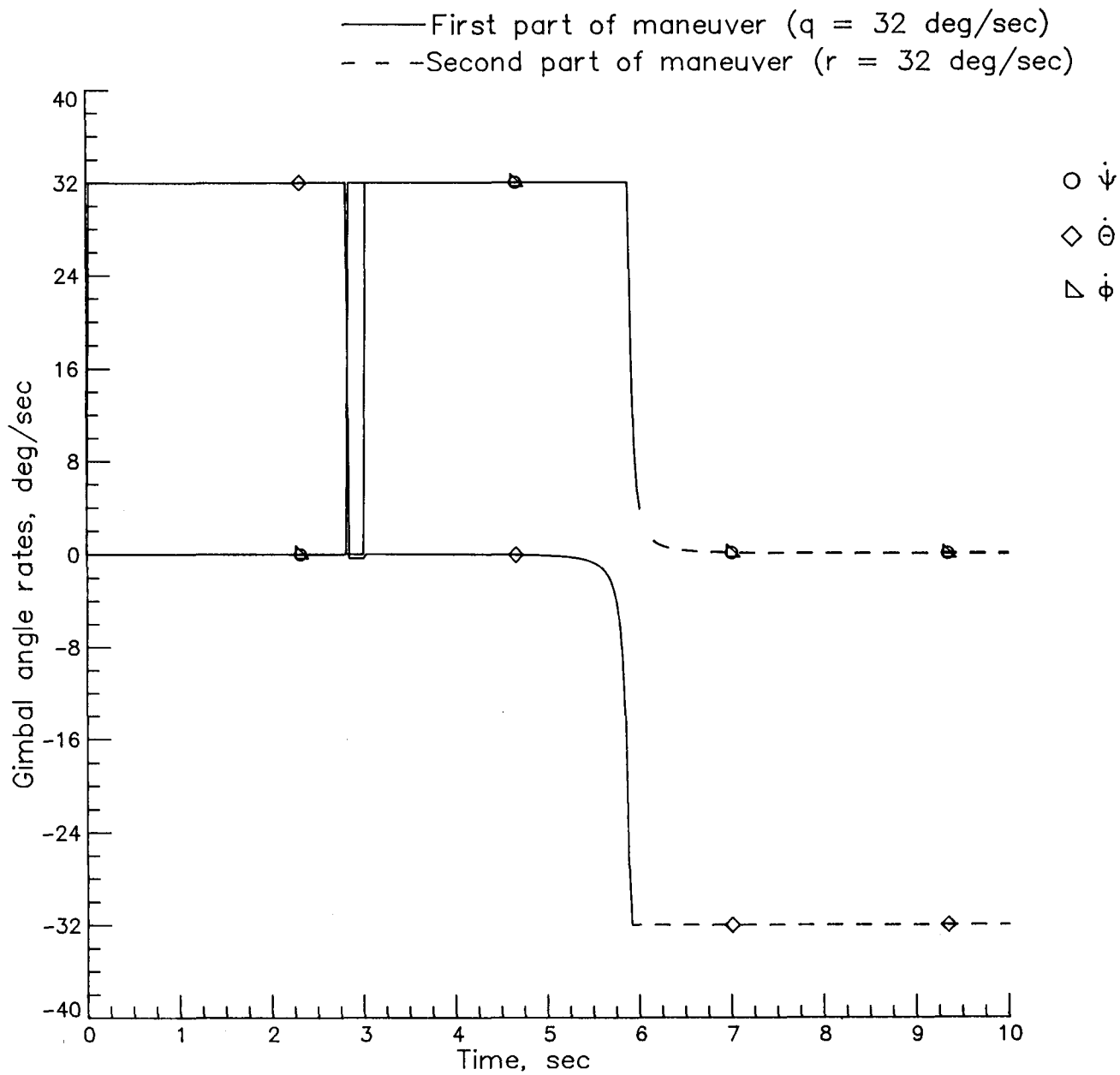
(c) Gimbal angle rates.

Figure 8. Continued.

(d) Gimbal angles.

Figure 8. Concluded.

(a) Operator inputs.

Figure 9. Basic test maneuver with four-gimbal robot wrist.
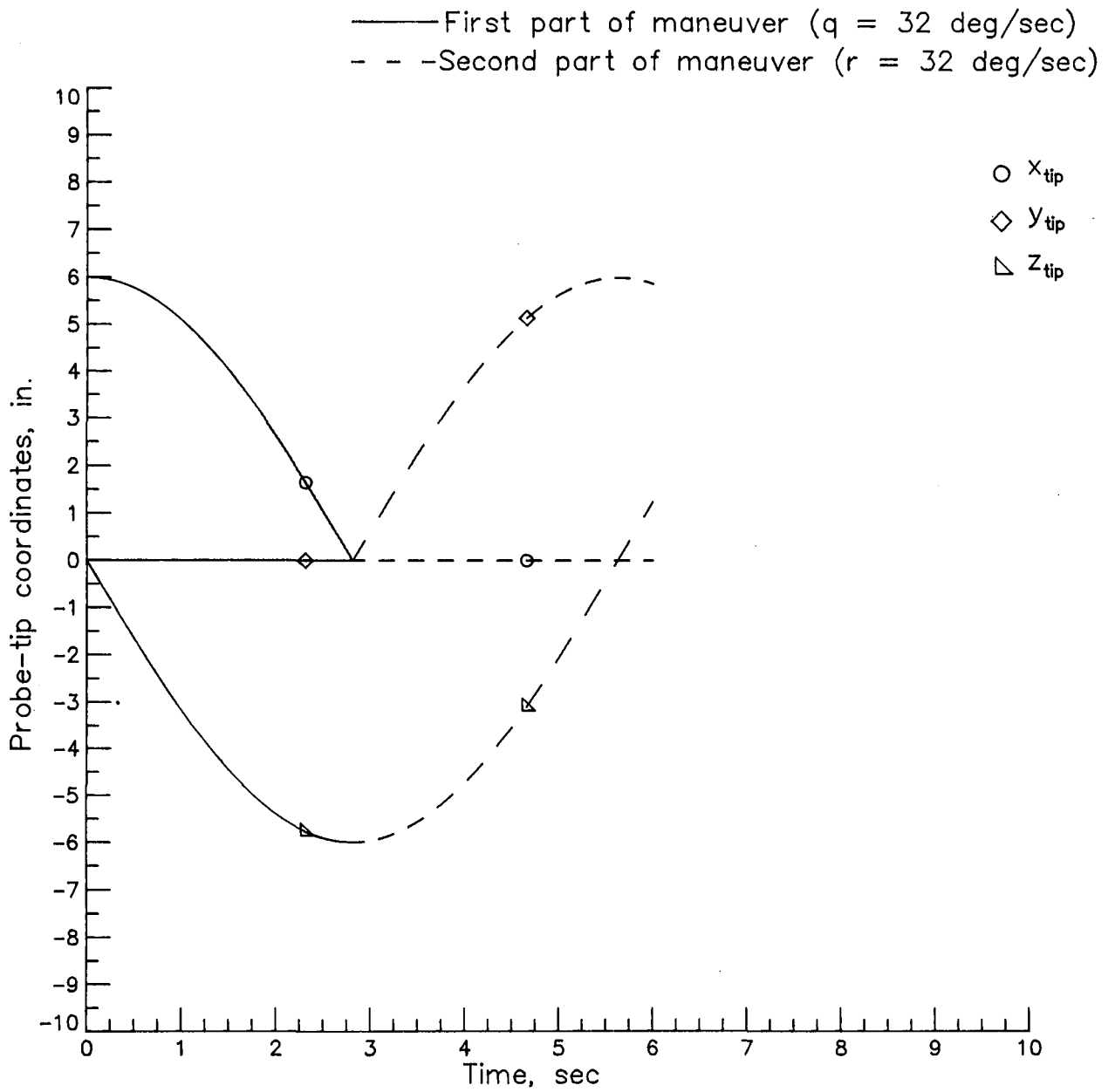
(b) Probe-tip movement.

Figure 9. Continued.

(c) Gimbal angle rates.

Figure 9. Continued.

(d) Gimbal angles.

Figure 9. Concluded.

(a) Operator inputs.

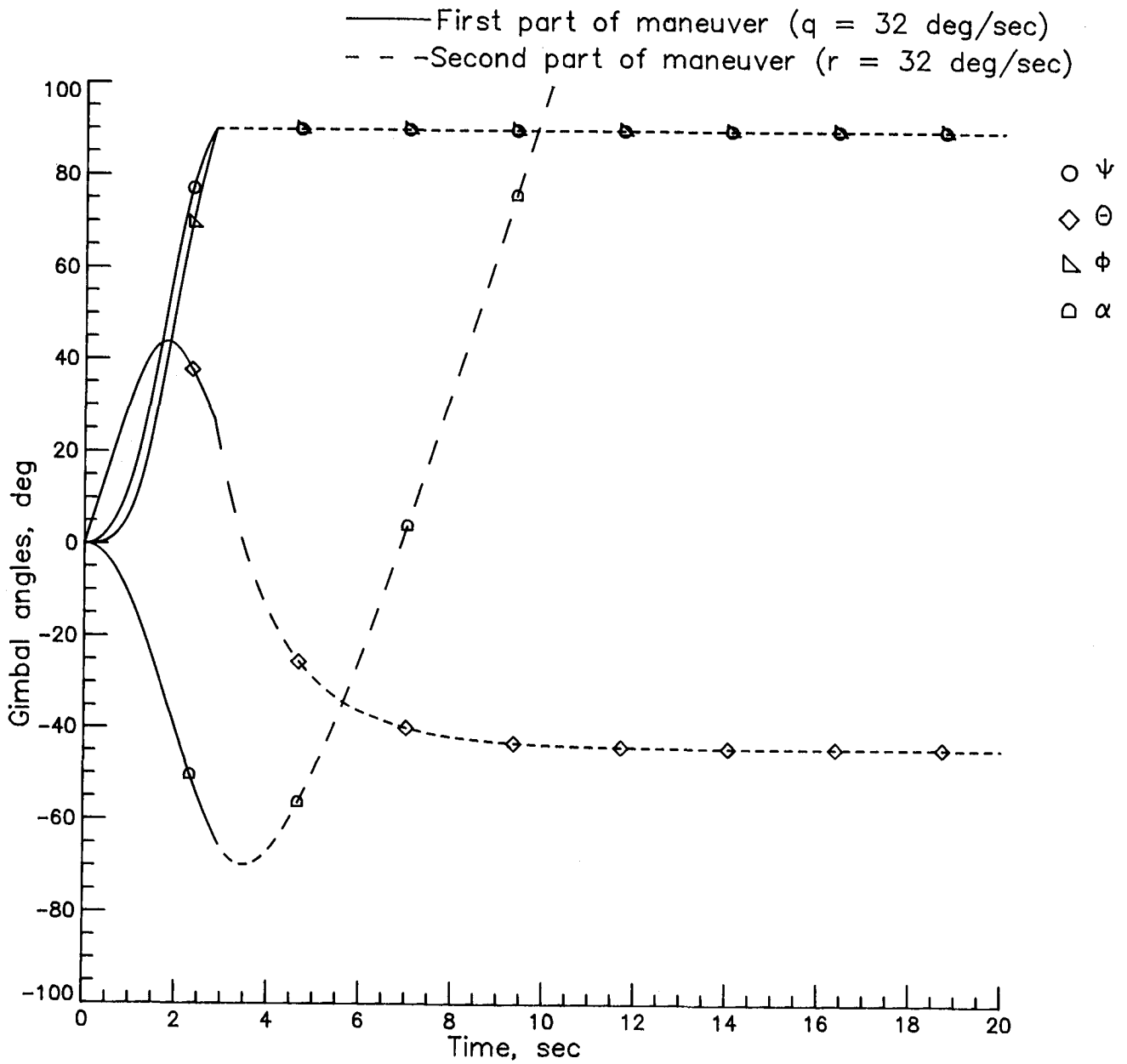Figure 10. Extended test maneuver with four-gimbal robot wrist. $K = 0.8$.
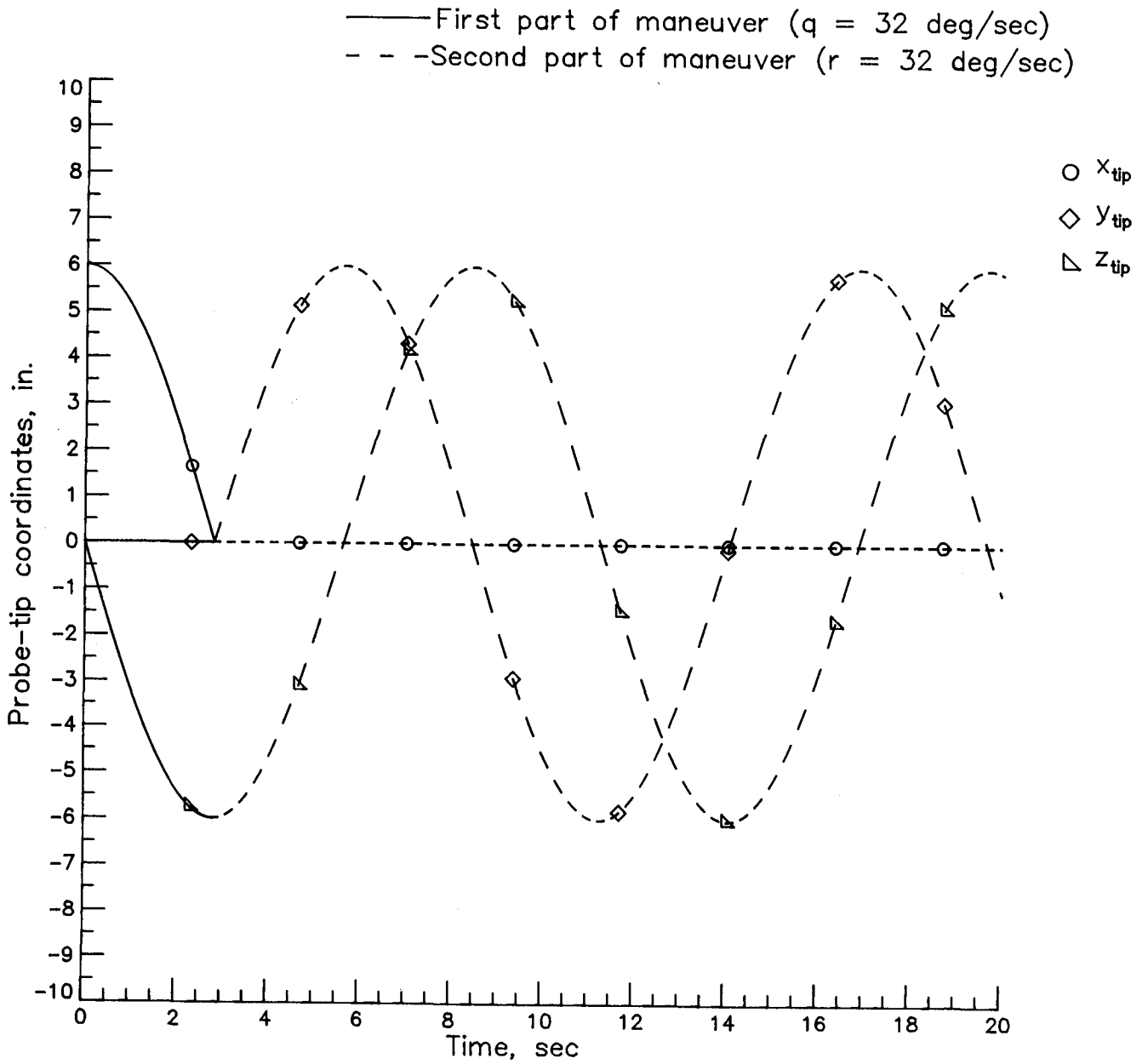
(b) Probe-tip movement.

Figure 10. Continued.

(c) Gimbal angle rates.

Figure 10. Continued.
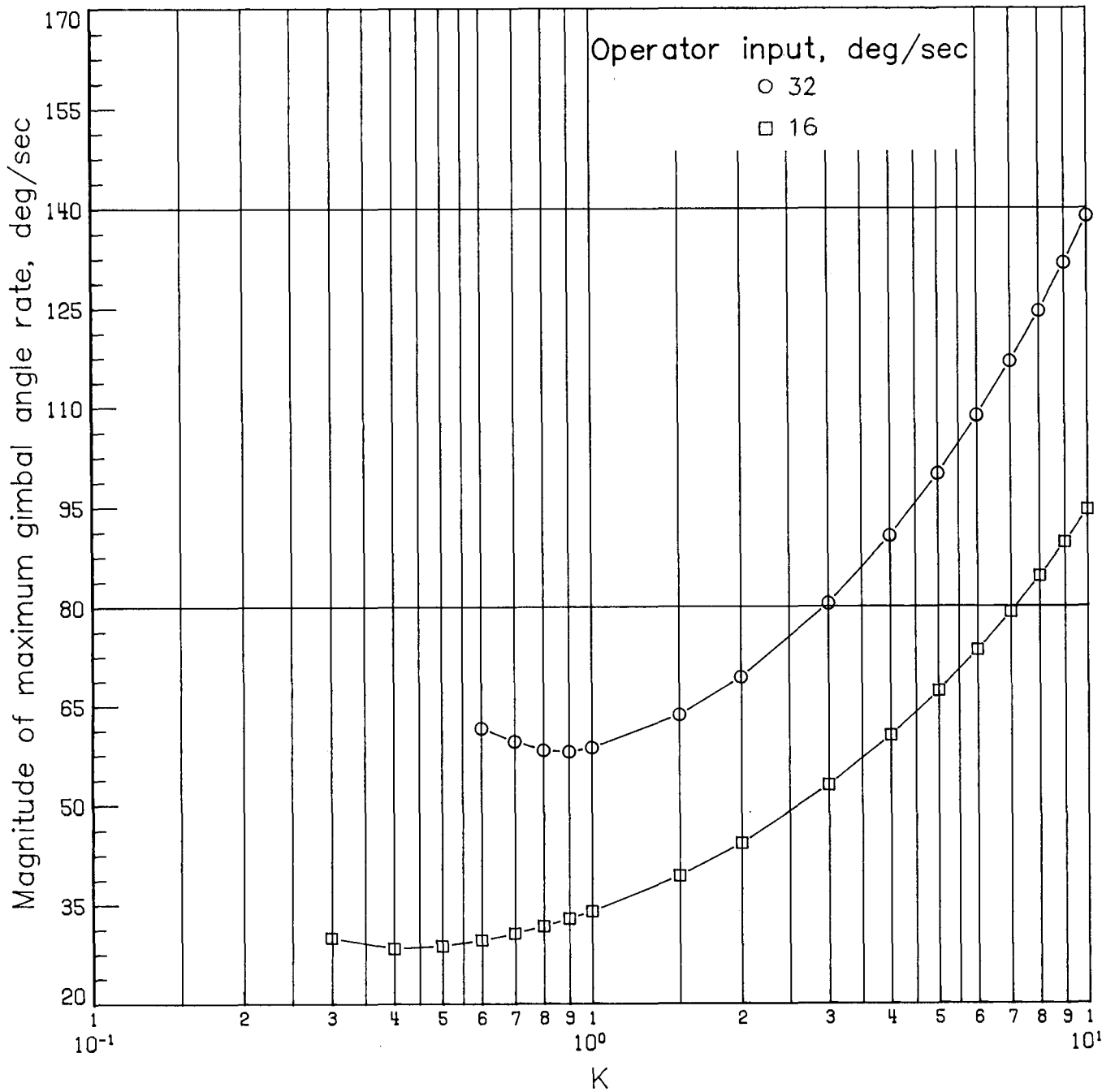
(d) Gimbal angles.

Figure 10. Concluded.

Figure 11. Magnitude of maximum gimbal angle rate encountered in extended test maneuver as function of gain K and operator input.

1. Report No. NASA TP-2564	2. Government Accession No.	3. Recipient's Catalog No.
4. Title and Subtitle Theoretical Three- and Four-Axis Gimbal Robot Wrists		5. Report Date May 1986
		6. Performing Organization Code 506-45-21-01
7. Author(s) L. Keith Barker and Jacob A. Houck		8. Performing Organization Report No. L-16042
9. Performing Organization Name and Address NASA Langley Research Center Hampton, VA 23665-5225		10. Work Unit No.
		11. Contract or Grant No.
12. Sponsoring Agency Name and Address National Aeronautics and Space Administration Washington, DC 20546-0001		13. Type of Report and Period Covered Technical Paper
		14. Sponsoring Agency Code

15. Supplementary Notes

16. Abstract

In high-performance flight simulations, a four-axis gimbal system allows all possible rotations with acceptable gimbal angle rates while it avoids the so-called "gimbal lock" that occurs when gimbal rotational axes are colinear. In this paper, pertinent equations (including quaternions) are assembled for a hypothetical robot wrist, functionally equivalent to this four-axis gimbal system, and also for a true three-axis gimbal robot wrist. These equations are used to simulate the rotation of a robot hand by the robot wrist in response to operator rotational velocity commands to the robot hand. Near gimbal lock (wrist singularity), excessive rotational rates occur. Scaling the rates, which is necessary for the three-gimbal robot wrist to prevent rate limiting, introduces an undesirable time delay in the robot hand rotation with respect to the commanded rotation. However, the merit of the four-gimbal robot wrist is that the fourth gimbal angle keeps the robot wrist away from the singularity so that the robot hand moves exactly as commanded. It appears that in a "worst-type" maneuver of the robot hand, the fourth gimbal angle can be defined so that none of the gimbal angle rates exceed about twice the commanded rates.

17. Key Words (Suggested by Authors(s)) Robot wrist Gimbal Four-axis robot wrist Singularity Three-axis robot wrist Resolved-rate control Flight simulation Quaternions	18. Distribution Statement Unclassified—Unlimited Subject Category 63

19. Security Classif.(of this report) Unclassified	20. Security Classif.(of this page) Unclassified	21. No. of Pages 36	22. Price A03

For sale by the National Technical Information Service, Springfield, Virginia 22161

National Aeronautics and
Space Administration
Code NIT-4

Washington, D.C.
20546-0001

NASA